Cortical bone distribution in the femoral neck of Paranthropus robustus

Marine Cazenave, José Braga, Anna Oettlé, Travis Rayne Pickering, Jason Heaton, Masato Nakatsukasa, J. Francis Thackeray, Frikkie de Beer, Jakobus Hoffman, Jean Dumoncel, et al.

Version of Record: https://www.sciencedirect.com/science/article/pii/S0047248418302392
Manuscript_b7cab3123203c859fc6c08cd858ec488

Cortical bone distribution in the proximal femoral neck of *Paranthropus robustus*

Marine Cazenave [a, b, c *], José Braga [b, d], Anna Oettlé [c, a], Travis R. Pickering [e, d, f], Jason L. Heaton [g, d, f], Masato Nakatsukasa [h], J. Francis Thackeray [d], Frikkie de Beer [i], Jakobus Hoffman [i], Jean Dumoncel [b], Roberto Macchiarelli [j, k]

[a] *Department of Anatomy, University of Pretoria, Pretoria, South Africa*

[b] *Computer-assisted Palaeoanthropology Team, UMR 5288 CNRS-Université Paul-Sabatier, Toulouse, France*

[c] *Department of Anatomy and Histology, Sefako Makgatho Health Sciences University, Ga-Rankuwa, Pretoria, South Africa*

[d] *Evolutionary Studies Institute and School of Geosciences, University of the Witwatersrand, Johannesburg, South Africa*

[e] *Department of Anthropology, University of Wisconsin, Madison, USA*

[f] *Plio-Pleistocene Palaeontology Section, Department of Vertebrates, Ditsong National Museum of Natural History (Transvaal Museum), Pretoria, South Africa*

[g] *Department of Biology, Birmingham-Southern College, Birmingham, USA*

[h] *Laboratory of Physical Anthropology, Department of Zoology, Graduate School of Science, Kyoto University, Kyoto, Japan*

[i] *South African Nuclear Energy Corporation SOC Ltd., Pelindaba, South Africa*

[j] *UMR 7194 CNRS-Muséum national d'Histoire naturelle, Musée de l'Homme, Paris, France*

[k] *Unité de Formation Géosciences, Université de Poitiers, Poitiers, France*

* Corresponding author.

E-mail address: marine.cazenave4@gmail.com (M. Cazenave).

ABSTRACT

Studies of the australopith (*Australopithecus* and *Paranthropus*) proximal femur have increasingly integrated information from the local arrangement of the cortical and cancellous bone to allow functional-biomechanical inferences on the locomotor behavioral patterns. In *Australopithecus africanus* and *Paranthropus robustus*, the cancellous bone organization at the center of the femoral head shows principal strut orientation similar to that of fossil and recent humans, which indicates that australopiths were human-like in many aspects of their bipedalism. However, by combining outer morphology with superoinferior asymmetry in cortical bone thickness at the base of neck and mid-neck, it has been suggested that, while adapted for terrestrial bipedality, australopiths displayed a slightly altered gait kinematics compared to *Homo*. We used techniques of 2D and 3D virtual imaging applied to an X-ray microtomographic record to assess cortical bone distribution along the entire femoral neck compartment in four upper femora from Swartkrans, South Africa (SK 82, SK 97, SK 3121, and SWT1/LB-2) and compared the results to the extant human and chimpanzee conditions. Our results support and extend previous evidence for more symmetric superior and inferior femoral neck cortical thicknesses in *P. robustus* than in modern humans and show that the differences are even greater than previously reported. However, *P. robustus* and humans still share a trend of lateral-to-medial decrease in asymmetry of the superior/inferior cortical thickness ratio, while this pattern is reversed in chimpanzees. We also identified two features uniquely characterizing *P. robustus*: an accentuated contrast between the relatively thicker anterior and the thinner posterior walls, and a more marked lateral-to-medial thinning of both cortices compared to extant humans and chimpanzees, which indicate wider interspecific differences among hominids in structural organization of the proximal femur than previously

reported. It remains to be ascertained if, and to what extent, these features also characterize the femoral neck of *Australopithecus*.

Cortical bone; Functional morphology; Hominin biomechanics; X-ray microtomography

1. Introduction

The anatomy of the proximal femur has been extensively investigated in the australopiths (the term subsuming here *Australopithecus* and *Paranthropus*) in order to reconstruct their locomotor repertoire (e.g., Lovejoy et al., 1973, 2002; Lovejoy, 1975, 1988; Ruff, 1995; Ohman et al., 1997; Ward, 2002, 2013; Ruff and Higgins, 2013; Ruff et al., 2016). Compared to the modern human condition, among other distinctive postcranial features, the australopith proximal femur shows a small head relative to the shaft breadth; a proportionally long and anteroposteriorly compressed neck (or, more appropriately, a superoinferiorly expanded neck relative to the femoral head breadth; Ruff and Higgins, 2013); a reduced neck-shaft angle; and a less laterally-projected greater trochanter positioned below the femoral head (e.g., Lovejoy et al., 1973; Lovejoy, 1975; McHenry, 1975; Tague and Lovejoy, 1986; Ruff, 1995, 2010; Ruff et al., 1999, 2016; Harmon, 2009; Berge and Goularas, 2010; Kibii et al., 2011; Ruff and Higgins, 2013). Such anatomy is associated with a relatively wide biacetabular breadth which appears to have characterized early hominin pelves (Gruss and Schmitt, 2015; Ruff, 2017; Vansickle, 2017). While it is still debated whether some morphological traits of the australopith hip joint evolved in response to functional demands or are retentions from an ancestral condition (Ward, 2013; Ruff et al., 2016), it has been shown that a complex and changing pattern of natural selection drove hominin hip and femoral evolution. In this context, many traits commonly suggested to have played functional roles in a bipedal gait evolved as a result of natural selection (Grabowski and Roseman, 2015).

While initially based entirely on the external morphology, studies of the australopith proximal femur have increasingly incorporated information from the internal bony structure, an analytical shift which has added critical elements for functional-biomechanical inferences on locomotor and behavioral patterns (Lovejoy, 1988; Ohman et al., 1997; Lovejoy et al., 2002; Ruff and Higgins, 2013; Chirchir et al., 2015; Ruff et al., 2016; Ryan et al., 2018; see also Ryan and Sukhdeo, 2016). Indeed, besides the influence of a number of biological (metabolic) factors on the inner bone organization and the imprint of a genetic component in the resulting evolutionary adaptive bauplan (e.g., Lovejoy et al., 1999; Judex et al., 2004; Demissie et al., 2007; Havill et al., 2007, 2010; Bonewald and Johnson, 2008; O'Neill and Dobson, 2008; Gosman et al., 2011; Wallace et al., 2012; Johansson et al., 2015), the mechanosensitive bone tissues remodel during life to adjust the loading environment (e.g., Huiskes, 2000; Lanyon and Skerry, 2001; Lieberman et al., 2003, 2004; Pearson and Lieberman, 2004; Mittra et al., 2005; Ruff et al., 2006; Skerry, 2008; Barak et al., 2011, 2017; Gosman et al., 2011; Raichlen et al., 2015). Accordingly, structural variation in femoral cortical and trabecular bone can be used as proxy for assessing hip joint loading and thus inferring functional behaviors in extant and extinct primates (e.g., Fajardo et al., 2007; Shaw and Ryan, 2012; Kivell, 2016; Ruff et al., 2016; Ryan et al., 2018).

Among the inner features of the hominin hip joint, the superoinferior asymmetry in cortical bone thickness at the femoral neck has been well studied (Ohman et al., 1997; Lovejoy et al., 2002; Ruff and Higgins, 2013; Ruff et al., 2016). Modern humans are characterized by a distinctly asymmetric distribution resulting from an absolutely thinner superior cortex and a thicker inferior cortex (Lovejoy, 1988, 2005; Ohman et al., 1997; Rafferty, 1998; Lovejoy et al., 2002; Ruff and Higgins, 2013; Ruff et al., 2016). The thinner superior cortex has been attributed to reduced strains in that region due to the action of the gluteal abductors producing a compressive force that counteracts tensile strains engendered by bending of the neck during

weight bearing (Lovejoy, 1988, 2005; Lovejoy et al., 2002; Ruff and Higgins, 2013; Ruff et al., 2016). Conversely, great apes possess a more symmetrical distribution of cortical bone across the neck (Ohman et al., 1997; Rafferty, 1998), possibly because of positioning, proportions and functioning of their gluteal muscles (Stern and Susman, 1981).

The human-like superoinferior asymmetry in cortical bone distribution across the femoral neck, as evidenced in *Australopithecus*, suggests a full commitment to terrestrial bipedalism (Ohman et al., 1997; Lovejoy et al., 2002). However, Ruff and Higgins (2013) showed that, especially at mid-neck, australopiths have relatively less asymmetric superior and inferior neck cortices than modern humans, while they are closer to modern human than nonhuman hominoids at the base of the neck (Ruff and Higgins, 2013). More recently, femoral neck cortical bone measures quantified on the *Australopithecus afarensis* A.L. 288-1 partial skeleton ('Lucy') support a pattern of breadth ratios that fall within but in the upper (i.e., more symmetric) portion of the modern human range, similar to some other australopith specimens (Ruff et al., 2016). However, the femoral neck is a 3D structure, thus its total inner structural arrangement cannot be completely captured by site-specific linear measurements, as is typically done. Additionally, while the superior/inferior cortical thickness ratio assessed at the base of neck and at mid-neck have received attention in primate comparative anatomy and paleoanthropology, limited data is available on the differences between anterior and posterior walls (Ohman et al., 1997) and, importantly, no study has yet quantified cortical bone distribution across the entire femoral neck in a fossil hominin taxon.

Here we apply 2D and 3D techniques of virtual imaging to assess the internal structural organization of the neck of four variably preserved proximal femora from Swartkrans, South Africa, attributed to *Paranthropus robustus* (SK 82, SK 97, SK 3121, and SWT1/LB-2). In this assemblage, SWT1/LB-2 is still unreported with regard to its inner structure (Pickering et al., 2012). By relying on a microtomographic (μXCT) record, we firstly aim to refine and expand

previous tomographic-based (XCT) measures of neck cortical bone thickness performed on SK 82 and SK 97 (Ruff and Higgins, 2013). Additionally, to furtherly evaluate the adaptive functional requirements having shaped the inner bony conformation of the hip joint in *P. robustus*, we provide the first evidence of cortical bone distribution and thickness proportions assessed in the entire femoral neck and compare these results with those from two samples representing *Homo sapiens* and *Pan troglodytes*.

According to Ohman et al. (1997), humans and African apes display generally uniform anterior and posterior cortical thicknesses along the neck and the cortices tend to slightly get thinner from the neck-shaft junction to the head, with little difference between the species. In addition, although anterior and posterior cortical bone topographic variation across the australopith femoral neck remains unknown, the anterior/posterior ratio assessed at approximately the neck-shaft junction in A.L. 288-1 is reported as indistinguishable from the human and ape conditions (Ohman et al., 1997). Accordingly, here we also test the hypothesis that also the *P. robustus* pattern is poorly distinguishable from both the human and the chimpanzee conditions.

2. Materials and Methods

2.1. Materials

Fossil specimens The investigated specimens, SK 82, SK 97, SK 3121, and SWT1/LB-2, all adults from the Pleistocene cave deposits of Swartkrans and curated at the Ditsong National Museum of Natural History, Pretoria, are shown in Figure 1.

SK 82 and SK 97 derive from the Hanging Remnant, while SWT1/LB-2 comes from the Lower Bank of the Member 1. According to cosmogenic nuclide burial dating (Gibbon et al., 2014), U/Pb dating of flowstone layers under- and overlying Member 1 (Pickering et al., 2011, 2019), and previous chronological estimates provided by Curnoe et al. (2001) and Balter et al.

(2008), as discussed by Herries et al. (2009), the most accurate chronology of Member 1 ranges between 2.31 and 1.64 Ma. Conversely, SK 3121 comes from the Member 2 breccia block, whose dating has proved more problematic. However, based on U-Pb dates (Balter et al., 2008; see also Herries et al., 2009; Gibbon et al., 2014), chronology of this unit should range between 1.36 and 1.1 Ma (Pickering et al., 2019), which is compatible with the biochronological framework assessed by Vrba (1975) and Delson (1988).

SK 82, discovered in 1949, represents a right proximal femur preserving the head (maximum diameter = 34.4 mm), the neck (mid-neck superoinferior diameter = 30.6 mm), the trochanteric region and 137 mm of shaft (Robinson, 1972). It is rather well preserved, but a fracture exists just at its head-neck junction. This specimen was attributed to *P. robustus* by Napier (1964), who was the first to identify and describe its non *Homo*-like morphology. Later, in attributing to *Paranthropus* the large majority (ca. 95%) of the taxonomically diagnostic craniodental material from Swartkrans Member 1, Grine (1989) provided support to Napier's original attribution. Based on its femoral head diameter compared to other specimens considered as conspecific, SK 82 likely represents a male individual (Susman et al., 2001). Estimated body mass in this individual is 37.1–45.3 kg (Pickering et al., 2012; Ruff et al., 2018).

SK 97, also discovered in 1949, is a right proximal femur preserving the head (maximum diameter = 38.4 mm), the neck (mid-neck superoinferior diameter = 30.9 mm), the trochanteric region, and 118 mm of shaft (Robinson, 1972). Similarly to SK 82, its neck is rather well preserved. However, two fractures run from the fovea capitis until the neck, where the specimen also shows a number of fine cracks. Attributed to *P. robustus* by Napier (1964; see also Grine, 1989) and very likely representing a male individual (Susman et al., 2001), SK 97 closely resembles to SK 82 in morphology, proportions, and cross-sectional geometry of the proximal shaft (Ruff et al., 1999; Ruff and Higgins, 2013). It has been noted that its greater and lesser trochanter approach the modern human morphology, even if some differences concern the

femoral tubercle which, differently from extant humans, is not clearly separate from the greater trochanter in SK 97, suggesting that the area of attachment for gluteus minimus extends slightly medialward than it occurs in *H. sapiens* (see Robinson, 1972). Estimated body mass in this individual is 43.2–53.8 kg (Pickering et al., 2012; Ruff et al., 2018).

SK 3121, discovered sometime before 1970, is a right proximal femur bearing ca. 23 mm of neck (mid-neck superoinferior diameter = 20.0 mm), notably along its upper margin. Within the assemblage of proximal femora attributed so far to *P. robustus*, SK 3121 displays the smallest articular end (maximum diameter = 29.9 mm), which supports its more likely attribution to a female individual. While incomplete, this specimen is relatively well preserved and its head-neck junction is rather smooth. According to Susman et al. (2001), the taxonomically most significant diagnostic feature of this fossil is represented by its anteroposteriorly compressed neck, a feature shared by all specimens investigated in the present study (Pickering et al., 2012). Estimated body mass in this individual is 24.1–30.0 kg (Pickering et al., 2012; Ruff et al., 2018).

SWT1/LB-2, discovered in 2010, represents a right proximal femur originally in two pieces (one composed of the head and neck and the other by a portion of the extreme proximal diaphysis truncated just inferior to the largely missing greater trochanter), but with a good contact between the two sections (Pickering et al., 2012). It preserves the head (maximum diameter = 35.2 mm), the neck (mid-neck superoinferior diameter = 27.4 mm) and a minor portion of the proximal diaphysis; however, it lacks most of the greater trochanter. The specimen's outer surface is well-preserved. Minor biochemical erosion is apparent in the form of a few localized, shallow linear features appearing on the cortex (Pickering et al., 2012). This fossil shows a relatively small head and an anteroposterior flatness of the long neck, which also probably had a low angle. Estimated body mass in this individual is 37.1–45.8 kg (Pickering et al., 2012; Ruff et al., 2018).

Comparative materials The extant human comparative sample consists of 25 femora from adult individuals (10 males and 15 females, aged from 21 to 54 years) of African and European ancestry selected from the McGregor Museum of Kimberley (*n* = 5; Morris, 1984), the Pretoria Bone Collection at the Department of Anatomy of the University of Pretoria (*n* = 16; L'Abbé et al., 2005), and the R.A. Dart skeletal collection at the University of the Witwatersrand (*n* = 4; Dayal et al., 2009), all in South Africa. Details on the composition of this diverse sample are provided as Supplementary Online Material (SOM) Table S1.

The *Pan troglodytes* sample (SOM Table S1) consists of 8 femora from 7 wild and one likely wild adult individuals of both sexes from the Evolutionary Studies Institute of the University of the Witwatersrand, Johannesburg (*n* = 1), the Muséum national d'Histoire naturelle of Paris, France (*n* = 2), and the Japan Monkey Center at Inuyama, Japan (*n* = 5; Shimizu et al., 2002).

All specimens used in this study for comparisons lack any macroscopic evidence of outer or inner alteration or obvious pathological changes.

2.2. Methods

Data acquisition and image processing To detail their inner structural morphology, all specimens were imaged by X-ray microtomography (µXCT). SK 82, SK 97, SK 3121 and SWT1/LB-2 were scanned between 2014 and 2017 at the microfocus X-ray tomography facility (MIXRAD) of the South African Nuclear Energy Corporation SOC Ltd (Necsa), Pelindaba, using a Nikon XTH 225 ST (Metris) equipment according to the following parameters: 100 kV (SK 3121 and SWT1/LB-2) and 190 kV (SK 82 and SK 97) tube voltage; 0.10 mA (SK 3121 and SWT1/LB-2) and 0.12 mA (SK 82 and SK 97) tube current; and an angular increment of 0.36° between each projection (for a total of 1000 projections). The final volumes were reconstructed with an isotropic voxel size ranging from 24 µm (SK 3121) to 79 µm (SK 82).

Sixteen extant human femora were also imaged at Necsa at resolutions ranging from 50 µm to 92 µm isotropic voxel size, while the remaining nine specimens forming the human reference sample were scanned at the X-ray microtomography facility of the University of the Witwatersrand at resolutions ranging from 50 µm to 70 µm isotropic voxel size (SOM Table S1).

The *Pan troglodytes* femora were scanned at resolutions ranging from 42 µm to 350 µm isotropic voxel size (the latter by using a SR light source) at the University of the Witwatersrand, the European Synchrotron Radiation Facility (ESRF) of Grenoble, France, and the National Science Museum of Tokyo, Japan (SOM Table S1).

By using the more complete SK 82 and SK 97 specimens as reference guide, SK 3121 and SWT1/LB-2 were virtually reoriented in Avizo v.8.0.0 software (Visualization Sciences Group Inc., Bordeaux) so that all were tentatively oriented in the same way. The images used to investigate the inner structural arrangement of the femoral neck were taken perpendicular to the main neck axis (Fig. 2). Independently from their original side, all extant comparative specimens were imaged as right femora. Repeated attempts performed to verify the degree of congruence of the virtually-oriented 2D and 3D reconstructions proved the reliability of the protocol.

Cortical bone analyses In SK 82, SK 97, SWT1/LB-2 and in all extant specimens used for comparison, the femoral neck was virtually delimited between the head-neck junction, medially, and its base, laterally, avoiding the superior flaring of the greater trochanter (Ruff and Higgins, 2013; Ruff et al., 2016). To extract its cortical shell from the deeper trabecular bone, a semiautomatic threshold-based segmentation with manual corrections (notably in the case of SK 82 and SWT1/LB-2) has been carried out (see the region-based segmentation approach based on topographic concepts known as the watershed transform, in Meyer and Beucher, 1990; Roerdink and Meijster, 2000) by Avizo v.8.0.0. In each specimen, the segmentation image stack

has been resliced perpendicular to the longitudinal neck axis to get the anteroposterior slices. To automatically assess all measurements, we used an ad hoc routine developed by J.D. using a program created with MATLAB v. 8.1 (MathWorks, 2013). For each reoriented segmentation slice, the most superior and inferior pixels of cortical bone were automatically detected to delimit the most superior (L1) and most inferior limits (L2) of the cortex, respectively (Fig. 3a). A superoinferior axis was defined as a line connecting the most superior and most inferior points (Ruff and Higgins, 2013). However, while in general we did not encounter difficulties in virtually extracting and assessing the neck cortex (Cazenave, 2015; Cazenave et al., 2015, 2017a), we could not reliably define the base of neck in SK 3121. Additionally, because of locally missing segments of bone and cracking (including across the lower endosteal border), the assessment of cortical bone thickness variation in SWT1/LB-2 was limited to its superior cortex and anterior neck wall (Fig. 4).

Whenever possible, the superior (S) and inferior (I) cortical thicknesses and their ratio (S/I) have been measured across the entire neck length. However, to allow direct comparisons with the results from other similar studies (Ruff and Higgins, 2013; Ruff et al., 2016), the local thicknesses measured at the base of neck and at mid-neck (Fig. 2) were specifically considered (for methodology, see Ruff and Higgins, 2013:Fig. 3). Additionally, to get a more comprehensive quantitative assessment of cortical bone topographic variation, in each slice perpendicular to the longitudinal axis of the virtually isolated femoral neck, the superior, inferior, anterior and posterior quadrants were delimited by two orthogonal lines set at 45° with respect to the superoinferior axis, and the average cortical thickness thus measured for each quadrant (Fig. 3b). For each pixel of the outer (periosteal) contour of the cortex, the thickness was defined as the smallest distance to the endosteal contour. Then, for each quadrant, the average of all measured thicknesses was calculated. For the anterior and posterior quadrants, the minimum and maximum thickness values were also measured. Intra- and interobserver

errors for accuracy of the repeated linear measurements (thicknesses) showed differences less than 4%.

Among the fossil sample, SK 82 preserves the best periosteal and endosteal neck surfaces. To provide a planar representation of cortical bone topographic thickness variation, we virtually unzipped the portion between the base of neck and the head-neck junction along a predefined line of its inferior aspect, unrolled such portion and projected its local properties into a morphometric map (Bondioli et al., 2010; see also Bayle et al., 2011; Morimoto et al., 2011; Puymerail et al., 2012; Jashashvili et al., 2015; Zanolli et al., 2018). The map was generated by a custom routine developed in R v.3.4.4 (R Core Team, 2018) with the packages Momocs (Bonhomme et al., 2014), spatstat (Baddeley et al., 2015) and gstat (Pebesma, 2004). Cortical bone thickness values have been standardized between 0 and 1 and the morphometric map has been set within a grid of 180 rows by 40 columns. To allow a comprehensive visual comparison between the structural signature characterizing SK 82 and the map summarizing the variation expressed by our extant human (n = 25) and chimpanzee (n = 8) samples, by a custom routine developed in Scilab Entreprises (2017) we performed generalized additive models (GAM) of interpolation by merging the individual morphometric maps into a single dataset to create a consensus map for each taxon (Wood, 2006; Puymerail et al., 2012).

3. Results

The virtual sections perpendicular to the longitudinal neck axis taken at the base of neck in SK 82, SK 97 and SWT1/LB-2 and at mid-neck in all four *P. robustus* specimens investigated here, including SK 3121, are shown in Figure 4 together with those of an extant human and a chimpanzee representative selected from our comparative samples.

Cortical bone thickness measures have been performed at the base of neck in SK 82, SK 97 and SWT1/LB-2 (only the upper cortex measured in the latter) and at mid-neck in SK 82, SK

97, SK 3121, and SWT1/LB-2 (again, only the upper cortex), respectively. Whenever possible, on the same virtual slices we also assessed the mean cortical thickness of the geometrically-defined superior and inferior quadrants (Fig. 3). The results are shown in Table 1, together with the XCT-based superior (S) and inferior (I) measurements previously performed on SK 82 and SK 97 by Ruff and Higgins (2013). Table 1 also shows the estimates obtained in our extant comparative samples, as well as the µXCT-based cortex thicknesses and ratios of the *A. afarensis* 'Lucy' (Ruff et al., 2016).

For SK 82 and SK 97, the differences between the µXCT-based (present study) and the XCT-based (Ruff and Higgins, 2013) measures vary between 0.54 mm (16.0%) and 1.12 mm (48.7%), at its base, and between 0.06 mm (2.1%) and 1.31 mm (46.6%), at mid-neck. In terms of polarity, those µXCT-based are higher (up to 1.12 mm) in five out of eight cases and lower (up to 0.58 mm) in the remaining three (Table 1). The impact of such differences on the S/I ratio of the two specimens is clear, as they imply less asymmetric cortices at the base of neck (0.76 vs. 0.47 and 0.68 vs. 0.42, in SK 82 and SK 97, respectively) and a closer signal between the two fossils for the mid-neck thickness ratio (0.86 vs. 1.05 and 0.96 vs. 0.68, in SK 82 and SK 97, respectively) than previously reported (Ruff and Higgins, 2013).

According to the present *P. robustus* estimates, the S/I cortical ratio varies from 0.68 (SK 97) to 0.76 (SK 82) at the base of neck, and from 0.71 (SK 3121) to 0.96 (SK 97) at mid-neck. Both mid-neck measures of the likely female specimen SK 3121 correspond to the absolutely thinnest cortices assessed within this fossil assemblage (no reliable measures available for SK 3121 at base of neck). For the S/I ratios assessed at both the base of neck and mid-neck, *P. robustus* is thus less asymmetric than measured in our extant human sample and also in 'Lucy' (Ruff, pers. comm.; see also Ruff et al., 2016:Fig. 7), but more asymmetric than *Pan troglodytes* at the base of neck (Table 1). Conversely, the average ratio at mid-neck measured in our

chimpanzee sample (0.66 ± 0.13) is comparable to the estimate of SK 3121 (0.71) but lower than assessed in both SK 82 (0.86) and SK 97 (0.96).

A rather coherent picture with respect to the pattern shown by the two linear measures taken at base of neck and mid-neck is provided by the mean cortical thickness assessed along the entire superior and inferior quadrants (Table 1; Fig. 3). In such case, however, while the likely female SK 3121 again shows the thinnest average superior cortex at mid-neck, that of the lower quadrant is shown by the likely male SK 82 (Table 1).

For SK 82 and SK 97, the standardized mediolateral variation of the S/I ratio from the base of neck (0%) to the head-neck junction (100%) is shown in Figure 5a and is compared to the extant human and chimpanzee variation expressed by our reference samples (Fig. 5b, c, respectively). As noted, SK 82 and SK 97 display more symmetric superior and inferior femoral neck cortical thicknesses than measured in extant humans. Yet, they share a tendency for a lateral-to-medial increase in this ratio, which in humans is especially accentuated across the medial half of the neck (Fig. 5b). Conversely, *Pan troglodytes* exhibits marked lateral-to-medial ratio decrease, i.e., a tendency towards thickness asymmetry inversion from the base of neck towards the femoral head (Fig. 5c).

We used quadrants also to compare mean cortical thickness variation across the anterior and posterior walls (Fig. 3). The results (Table 2; Fig. 6) are shown for SK 82, SK 97 and SWT1/LB-2 (the latter uniquely considered for its anterior wall) and for the extant human and chimpanzee samples. The fossils SK 82 and SK 97 evince thicker anterior and thinner posterior walls across the entire neck (Fig. 6a, b), while cortex asymmetry is nearly absent in extant humans (Fig. 6d, e) and is modest in chimpanzees, the average anterior wall measured in our sample being only slightly thicker (Fig. 6f, g). Differently from the S/I ratio (Fig. 5), the tendency in *P. robustus* and, to a lesser extent, in extant humans and *Pan*, is towards a lateral-to-medial decrease of the

average cortical thickness across both walls. Among the three fossil specimens, SWT1/LB-2 shows, on average, the thickest anterior wall (Table 2; Fig. 6c).

The standardized morphometric maps of the virtually projected cortical bone thickness of the SK 82's neck and the consensus cartographies generated for the extant human and chimpanzee samples are shown in Figure 7. It should be noted that, similarly to the results provided in Figure 5 for the S/I ratio and in Figure 6 for the anterior vs. posterior wall thickness variation, the geometrically-defined quadrants are neck shape-dependent. Thus, the morphometric maps provide information derived from surfaces having slightly different proportions in each taxon. When compared to the average human condition, for example, the superior quadrant of *P. robustus* is longer and narrower, while its anterior wall is both laterally-to-medially and superoinferiorly more extended.

In terms of both relative topographic distribution pattern and absolute cortex thickness, the contrast between SK 82, dominated by 'warm-hot' colors, and the extant human consensus map, where 'cool' dark blue associated to thinner cortex is spread, is especially marked, notably for the superior and anterior neck quadrants. As rendered by the pseudocolor scale, an intermediate pattern, or cortices locally as thick as measured in *P. robustus*, are displayed by *Pan troglodytes* (Table 2), whose consensus map is dominated by green-cyan to yellow 'warm' colors. In all three taxa, a variably expressed trend of lateral-to-medial cortical thinning (bottom-top direction in each map of Fig. 7) is found within all neck quadrants.

4. Discussion

The internal organization of the hominid proximal femur is seen as intimately related to variation in hip joint loading (Ohman et al., 1997; Rafferty, 1998; Lovejoy et al., 2002; Ruff and Higgins, 2013; Chirchir et al., 2015; Ruff et al., 2016; Ryan et al., 2018). With regard to the femoral neck, in extant humans cortical bone is estimated to carry from ca. 50% to ca. 96%

of the loads at the mid-neck and base of the neck, respectively, i.e., considerably more than the subcapital region (ca. 20%; Lotz et al. 1995). Nonetheless, quantitative evidence available so far on cortex variation across the femoral neck in nonhuman fossil hominin taxa remains limited (Lovejoy, 1988; Ohman et al., 1997; Lovejoy et al., 2002; Ruff and Higgins, 2013; Marchi et al., 2016; Ruff et al., 2016; DeSilva et al., 2018; Simpson et al., 2019). Using the assemblage of four proximal femora from Swartkrans currently attributed to *P. robustus* (SK 82, SK 97, SK 3121, and SWT1/LB-2), we refined some local estimates of the degree of superior vs. inferior cortical bone thickness asymmetry of the neck in this taxon (Ruff and Higgins, 2013). In addition, we extended such 2D and 3D analyses to the entire compartment, in order to verify if *P. robustus* also aligns with the general structural pattern of rather uniform anterior and posterior cortical thickness distribution along the neck and of slight lateral-to-medial thinning suggested to be shared by humans and African apes, with little interspecific differences (Ohman et al., 1997).

Major limitations in our study were imposed by the incompleteness of the fossil specimens (notably, SK 3121) and the heterogeneous preservation quality of their inner signal (notably, the posterior and inferior cortices in SWT1/LB-2). In the present and other similar studies, the current lack of comparative evidence from *Pan paniscus* represents another limiting factor because of the possibility that, even if minor, some differences in locomotor behavior observed between chimpanzees and bonobos in arboreal travel component and function or use of bipedality (e.g., Doran, 1993; Videan and McGrew, 2001) may be also recorded at the hip joint in terms of endostructural bony arrangement. Nonetheless, our results provide a rather coherent picture of some unique features characterizing *P. robustus* with respect to both the extant human and chimpanzee patterns which may have implications in the reconstruction of the hip joint loading conditions in this fossil hominin taxon.

As noted, compared to the modern human condition, the australopith femoral neck is longer and superoinferiorly expanded relative to the femoral head breadth (reviewed in Ruff and Higgins, 2013). Asymmetry in cortical bone thickness distribution between the superior and inferior margins, the former being absolutely thinner, is considered a typical human structural feature developed as mechanical response to the more stereotypic loading pattern imposed by habitual bipedal locomotion and the action of the gluteal abductor muscles, which is also variably expressed in australopiths (Lovejoy, 1988, 2005; Ohman et al., 1997; Rafferty, 1998; Lovejoy et al., 2002; Ruff and Higgins, 2013; Ruff et al., 2016). Our new set of higher resolution measures at the base and mid-neck confirm that *P. robustus* displays a thicker inferior cortex, especially laterally, which supports the view of a human-like action of the gluteal abductors producing a compressive force counteracting the tensile strains in the superior cortex (Lovejoy et al., 2002; Ruff and Higgins, 2013). However, while still consistent in terms of pattern, they also provide evidence for more symmetric superior and inferior femoral neck cortical thicknesses in *P. robustus* than in modern humans than previously reported using an XCT-based record (Ruff and Higgins, 2013). Besides possible slight variations between the studies in positioning or orientation of the mid-neck and base of neck sections, reasons for such differences more likely depend on the higher resolution of the µXCT record used in the present study, i.e., about ×3 better in the section plane (79 µm and 70 µm vs. 230 µm for SK 82 and SK 97, respectively). In any case, even if at this stage the functional meaning of a lower degree of asymmetry between the superior and inferior cortices remains to be ascertained, these results tend to support the possible existence of slight differences in cortical bone distribution asymmetry across the femoral neck between *P. robustus* (less asymmetric) and *A. afarensis* (more asymmetric), at least as documented so far in the latter taxon by the two specimens MAK VP-1/1 (Ohman et al., 1997; Lovejoy et al., 2002) and A.L. 288-1 (Ruff et al., 2016), whose asymmetry pattern would more closely approach the human condition. While a number of

mechanical, anatomical and physiological factors may account for a less humanlike pattern displayed by *P. robustus* compared to *A. afarensis* (e.g., actual differences in gait mechanics related to non-fully overlapping ranges of locomotor performances, differences in relative muscular development and attachment areas at the hip joint, age- and/or sex-related differences in body size and shape among the few individuals investigated so far, the influence of hormones on bone growth and maintenance), it should be acknowledged that current evidence, particularly from *Australopithecus*, remains extremely scanty.

Paranthropus robustus shows a human-like trend of lateral-to-medial asymmetry decrease of the superior/inferior cortical thickness ratio from the base of neck to the head-neck junction, while this pattern is uniquely reversed in chimpanzees. Here, the only likely female *P. robustus* specimen available for measurements at the base of neck and mid-neck (SK 3121) shows absolutely thinner cortices compared to the likely males (SK 82, SK 97 and SWT1/LB-2). However, as also recorded at other sites of the postcranial skeleton (e.g., Ruff et al., 1999; Bleuze, 2010; Domínguez-Rodrigo et al., 2013; Dowdeswell et al., 2016; Cazenave et al., 2017b, 2019), cortical bone at the femoral neck is globally thicker in *P. robustus* than in humans, the small *Pan troglodytes* sample used in this study revealing intermediate values across the entire compartment, or cortices locally as thick as in *P. robustus*.

Differently from the uniquely derived hominin pattern of superior/inferior cortical asymmetry, previous XCT-based observations performed by Ohman et al. (1997) suggest that humans and African apes share a rather uniform cortical bone thickness distribution between the anterior and posterior walls of the femoral neck in association to a pattern of slight lateral-to-medial thinning. Our 2D (Fig. 6) and 3D (Fig. 7) analyses confirm that cortical asymmetry is absent in the extant human and poorly expressed/absent also in chimpanzees. However, they also show a previously unreported morphology: while sharing with both humans and chimpanzees a tendency towards a lateral-to-medial decrease in average cortical thickness

across both walls, two *P. robustus* specimens (SK 82 and SK 97) reveal a relatively thicker anterior wall, especially within the lateral and central portions of the femoral neck (Figs. 6 and 7). Due to incomplete preservation, no reliable information is available for the entire posterior wall of SWT1/LB-2. Nonetheless, we note that this specimen possesses the absolutely thickest anterior cortex recorded in the present study (Table 2; Fig. 6c).

Following Ruff and Higgins (2013), the condition of variably less asymmetric cortices in the australopith femoral neck compared to humans points to a relative increase in superoinferior bending of the neck likely associated with a greater lateral displacement of the body center of gravity over the stance limb during the support phase of gait. This condition engenders a more vertical hip joint reaction force and bending increase relative to the neck axial loadings (Ruff and Higgins, 2013). Such loading conditions are compatible with a superoinferior, not an anteroposterior, expansion of the femoral neck, which is a typical australopith feature. Accordingly, it is likely that in australopiths "anterior and posterior strains decline under a more vertical loading configuration" (Ruff and Higgins, 2013:521). The thicker anterior wall detected in at least two *P. robustus* representatives lacking in humans and absent/poorly expressed in African apes (Ohman et al., 1997, and present results on *Pan troglodytes*), could precisely result from the unique australopith architecture combining a longer, superoinferiorly expanded and anteroposteriorly relatively compressed femoral neck. In terms of quadrant proportions, compared to the extant human pattern, the australopith neck conformation implies mediolaterally extended but absolutely narrower superior and inferior bone surfaces, a greater portion of compressive loads being thus absorbed through anterior cortex thickening. If so, it is expected that the structural neck conformation in *Australopithecus* resembles that of *P. robustus* in the degree of anterior vs. posterior wall thickness asymmetry more closely than measured in extant humans and chimpanzees. Alternatively, whenever the inner organization of *Australopithecus* is closer to the human pattern, or even reveals another configuration, it would

imply different hip joint loading conditions in the two extinct hominins likely resulting from non-fully overlapping locomotor modes.

5. Conclusions

Cortical bone distribution quantitatively assessed along the entire femoral neck compartment revealed a number of features uniquely distinguishing *P. robustus* with respect to extant humans and chimpanzees and, at least for the degree of asymmetry in cortex thickness measured between the superior and inferior margins, also to *A. afarensis*, which seems to more closely approach the human condition for this ratio. With respect to previous studies of the hominin proximal femoral end, our analyses show that, in addition to absolutely thick cortices, *P. robustus* displays a pattern combining relatively thicker anterior and thinner posterior walls across the entire neck, while cortex asymmetry between these two walls is hardly appreciable in extant humans and is also faint in chimpanzees. So far, the condition characterizing *Australopithecus* is unknown.

As suggested by previous research, Plio-Pleistocene hominins practiced different forms of terrestrial bipedality (e.g., Stern, 2000; Ward, 2002, 2013; Lovejoy et al., 2009; Haile-Selassie et al., 2012; Barak et al., 2013; DeSilva et al., 2012, 2013; Harcourt-Smith, 2016; Ruff et al., 2016, 2018; Zeininger et al., 2016), likely implying slightly different gait kinematics (Komza and Skinner, 2019). Evidence for some variations between *A. africanus* and *Paranthropus* has been provided by the study of the trabecular architecture of the hip bone (Macchiarelli et al., 1999) and of the talus (Su and Carlson, 2017), while no textural differences have been found between the two taxa at the femoral head (Ryan et al., 2018). Based on the results of the present study, we predict that a refined comparative assessment of the australopith inner structural organization of the femoral neck (Ruff et al., 2016; Ryan et al., 2018) has the potential to reveal gait-related subtle differences possibly distinguishing *Australopithecus* and *Paranthropus*. In

this perspective, it will be essential to preliminarily characterize and compare for possible topographic differences the cortical bone distribution patterns at the femoral neck in *Pan troglodytes* and *Pan paniscus*.

Acknowledgements

For access to fossil and comparative materials, we are grateful to the curatorial staff of the Ditsong National Museum of Natural History, Pretoria; the Pretoria Bone Collection at the Department of Anatomy of the University of Pretoria; the Evolutionary Studies Institute at the University of the Witwatersrand, Johannesburg; the McGregor Museum of Kimberley; and the Muséum national d'Histoire naturelle, Paris and M. Nakamura (Kyoto) and Y. Shintaku (Inuyama) for permission/help to access Mahale chimpanzee collection. For the extant human comparative sample, ethical clearance was obtained from the Faculty of Health Sciences Research Ethics committee of the University of Pretoria (ref. no. 39/2016). We especially acknowledge B. Billing (Johannesburg), L. Kgasi (Pretoria), D. Morris (Kimberley), S. Potze (Pretoria), M. Tawane (Pretoria) and B. Zipfel (Johannesburg). We also thank K. Jakata (Johannesburg), L. Bam (Pelindaba) and R. Kono (Yokohama) for X-ray micro-tomographies at Wits, Necsa and Tokyo, respectively. Acquisitions at the ESRF were performed by R.M. within the EC TNT project in collaboration with A. Mazurier (Poitiers). For scientific collaboration and generous availability to run independent measures for inter-observer error assessment, we thank A. Beaudet (Johannesburg), A. Mazurier and C. Zanolli (Bordeaux). For data sharing, we thank C.B. Ruff (Baltimore). For discussion, we thank A. Beaudet, L. Bruxelles (Johannesburg and Toulouse), K. Carlson (Johannesburg and Los Angeles), R.J. Clarke (Johannesburg), F.E. Grine (Stony Brook), T. Jashashvili (Johannesburg and Los Angeles), D. Marchi (Pisa), E. Pouydebat (Paris), C. Zanolli and B. Zipfel. M.C. especially thanks T.L. Kivell and M.M. Skinner for comments (Canterbury). Finally, we are grateful to

David Alba, the Associate Editor, and to four anonymous reviewers for constructive critique that considerably improved this manuscript. We acknowledge the DST-NRF for financial support (Grant # UID23456) to establish the MIXRAD microfocus X-ray tomography facility at Necsa. M.C. was funded by the European Commission (EACEA), Erasmus Mundus programme, AESOP and AESOP+ consortia coordinated by J.B and by the Erasmus Mundus programme, Bakeng se Afrika.

References

Baddeley, A., Rubak, E., Turner, R., 2015. Spatial Point Patterns: Methodology and Applications with R. Chapman and Hall/CRC Press, London.

Balter, V., Blichert-Toft, J., Braga, J., Telouk, P., Thackeray, F., Albarède, F., 2008. U-Pb dating of fossil enamel from the Swartkrans Pleistocene hominid site, South Africa. Earth and Planetary Science Letters 267, 236-246.

Barak, M.M., Lieberman, D.E., Hublin, J.J., 2011. A Wolff in sheep's clothing: Trabecular bone adaptation in response to changes in joint loading orientation. Bone 49, 1141-1151.

Barak, M.M., Lieberman, D.E., Raichlen, D., Pontzer, H., Warrener, A.G., Hublin, J.J., 2013. Trabecular evidence for a human-like gait in *Australopithecus africanus*. PLoS One 8, e77687.

Barak, M.M., Sherratt, E., Lieberman, D.E., 2017. Using principal trabecular orientation to differentiate joint loading orientation in the 3rd metacarpal heads of humans and chimpanzees. Journal of Human Evolution 113, 173-182.

Bayle, P., Bondioli, L., Macchiarelli, R., Mazurier, A., Puymerail, L., Volpato, V., Zanolli, C., 2011. Three-dimensional imaging and quantitative characterization of human fossil remains. Examples from the NESPOS database. In: Macchiarelli, R., Weniger, G.-C. (Eds),

Pleistocene Databases. Acquisition, Storing, Sharing, vol. 4. Wissenschaftliche Schriften des Neanderthal Museums, Mettmann, pp. 29-46.

Berge, C., Goularas, D., 2010. A new reconstruction of Sts 14 pelvis (*Australopithecus africanus*) from computed tomography and three-dimensional modeling techniques. Journal of Human Evolution 58, 262-272.

Bleuze, M.M., 2010. Cross-sectional morphology and mechanical loading in Plio-Pleistocene hominins: Implications for locomotion and taxonomy. Ph.D. Dissertation, The University of Western Ontario.

Bondioli, L., Bayle, P., Dean, C., Mazurier, A., Puymerail, L., Ruff, C., Stock, J.T., Volpato, V., Zanolli, C., Macchiarelli, R., 2010. Morphometric maps of long bone shafts and dental roots for imaging topographic thickness variation. American Journal of Physical Anthropology 142, 328-334.

Bonewald, L.F., Johnson, M.L., 2008. Osteocytes, mechanosensing and Wnt signaling. Bone 42, 606-615.

Bonhomme, V., Picq, S., Gaucherel, C., Claude, J., 2014. Momocs: outline analysis using R. Journal of Statistical Software 56, 1-24.

Cazenave, M., 2015. The inner structural morphology of the femoral head of *Paranthropus robustus*. Master Thesis, Université Toulouse III - Paul Sabatier.

Cazenave, M., Braga, J., de Beer, F., Hoffman, J.W., Macchiarelli, R., Thackeray, J.F., 2015. The inner structural morphology of the femoral head of *Paranthropus robustus*. Proceedings of the European Society for the Study of Human Evolution 5, 68.

Cazenave, M., Braga, J., de Beer, F., Hoffman, J.W., Macchiarelli, R., Oettlé, A., Thackeray, J.F., 2017a. Site-specific cortical bone topographic variation across the whole neck assessed in two hominin proximal femora from Swartkrans Member 1, South Africa: SK 82 and SK 97. American Journal of Physical Anthropology 162, S64, 140.

Cazenave, M., Braga, J., Oettlé, A., Thackeray, J.F., de Beer, F., Hoffman, J., Endalamaw, M., Engda Redae, B., Puymerail L., Macchiarelli, R., 2017b. Inner structural organization of the distal humerus in *Paranthropus* and *Homo*. In: Macchiarelli, R., Zanolli, C. (Eds), Hominin Biomechanics, Virtual Anatomy and Inner Structural Morphology: From Head to Toe. A Tribute to Laurent Puymerail. Comptes Rendus Palevol 16, 521-532.

Cazenave, M., Oettlé, A., Thackeray, J.F., Nakatsukasa, M., de Beer, F., Hoffman, J., Macchiarelli, R., 2019. The SKX 1084 hominin patella from Swartkrans Member 2, South Africa: An integrated analysis of its outer morphology and inner structure. Comptes Rendus Palevol 18, 223-235.

Chirchir, H., Kivell, T.L., Ruff, C.B., Hublin, J.-J., Carlson, K.J., Zipfel, B., Richmond, B.G., 2015. Recent origin of low trabecular bone density in modern humans. Proceedings of the National Academy of Sciences USA 112, 366-371.

Curnoe, D., Grün, R., Taylor, L., Thackeray, F., 2001. Direct ESR dating of a Pliocene hominin from Swartkrans. Journal of Human Evolution 40, 379-391.

Dayal, M.R., Kegley, A.D.T., Štrkalj, G., Bidmos, M.A., Kuykendall, K.L., 2009. The history and composition of the Raymond A. Dart collection of human skeletons at the University of the Witwatersrand, Johannesburg, South Africa. American Journal of Physical Anthropology 140, 324-335.

Delson, E., 1988. Chronology of South African australopith site units. In: Grine, F.E. (Ed.), Evolutionary History of the "Robust" Australopithecines. Aldine de Gruyter, New York, pp. 317-324.

Demissie, S., Dupuis, J., Cupples, L.A., Beck, T., Kiel, D.P., Karasik, D., 2007. Proximal hip geometry is linked to several chromosomal regions: Genome-wide linkage results from the Framingham Osteoporosis Study. Bone 40, 743-750.

DeSilva, J.M., Devlin, M.J., 2012. A comparative study of the trabecular bony architecture of the talus in humans, non-human primates, and *Australopithecus*. Journal of Human Evolution 63, 536-551.

DeSilva, J.M., Holt, K., Churchill, S., Carlson, K., Walker, C., Zipfel, B., Berger, L., 2013. The lower limb and mechanics of walking in *Australopithecus sediba*. Science 340, 1232999.

DeSilva, J.M., Carlson, K.J., Claxton, A.G., Harcourt-Smith, W.E., McNutt, E.J., Sylvester, A.D., Walker, C.S., Zipfel, B., Churchill, S.E., Berger, L., 2018. The anatomy of the lower limb skeleton of *Australopithecus sediba*. PaleoAnthropology 2018, 357-405.

Doran, D.M., 1993. Comparative locomotor behavior of chimpanzees and bonobos: The influence of morphology on locomotion. American Journal of Physical Anthropology 91, 83-98.

Domínguez-Rodrigo, M., Pickering, T.R., Baquedano, E., Mabulla, A., Mark, D.F., Musiba, C., Pérez-González, A., 2013. First partial skeleton of a 1.34-million-year-old *Paranthropus boisei* from Bed II, Olduvai Gorge, Tanzania. PLoS One 8, e80347.

Dowdeswell, M.R., Jashashvili, T., Patel, B.A., Lebrun, R., Susman, R.L., Lordkipanidze, D., Carlson, K.J., 2016. Adaptation to bipedal gait and fifth metatarsal structural properties in *Australopithecus*, *Paranthropus*, and *Homo*. In: Macchiarelli, R., Zanolli, C. (Eds), Hominin Biomechanics, Virtual Anatomy and Inner Structural Morphology: From Head to Toe. A Tribute to Laurent Puymerail. Comptes Rendus Palevol 16, 585-599.

Fajardo, R.J., Müller, R., Ketcham, R.A., Colbert, M., 2007. Nonhuman anthropoid primate femoral neck trabecular architecture and its relationship to locomotor mode. The Anatomical Record 290, 422-436.

Gibbon, R.J., Rayne, T., Sutton, M.B., Heaton, J.L., Kuman, K., Clarke, R.J., Brain, C.K., Granger, D.E., 2014. Quaternary geochronology cosmogenic nuclide burial dating of

hominin-bearing Pleistocene cave deposits at Swartkrans, South Africa. Quaternary Geochronology 24, 10-15.

Gosman, J.H., Stout, S.D., Larsen, C.S., 2011. Skeletal biology over the life span: A view from the surfaces. American Journal of Physical Anthropology 146, 86-98.

Grabowski, M.W., Roseman, C.C., 2015. Complex and changing patterns of natural selection explain the evolution of the human hip. Journal of Human Evolution 85, 94-110.

Grine, F.E., 1989. New hominid fossils from the Swartkrans formation (1979-1986 excavations): Craniodental specimens. American Journal of Physical Anthropology 79, 409-449.

Gruss, L.T., Schmitt, D., 2015. The evolution of the human pelvis: Changing adaptations to bipedalism, obstetrics and thermoregulation. Philosophical Transactions of the Royal Society B 370, 20140063.

Haile-Selassie, Y., Saylor, B., Deino, A., Levin, N., Alene, M., Latimer, B., 2012. A new hominin foot from Ethiopia shows multiple Pliocene bipedal adaptations. Nature 483, 565-569.

Harcourt-Smith, W., 2016. Early hominin diversity and the emergence of the genus *Homo*. Journal of Anthropological Sciences 94, 19-27.

Harmon, E., 2009. Size and shape variation in the proximal femur of *Australopithecus africanus*. Journal of Human Evolution 56, 551-559.

Havill, L.M., Allen, M.R., Bredbenner, T.L., Burr, D.B., Nicolella, D.P., Turner, C.H., Warren, D.M., Mahaney, M.C., 2010. Heritability of lumbar trabecular bone mechanical properties in baboons. Bone 46, 835-840.

Havill, L.M., Mahaney, M.C., Binkley, T.L., Specker, B.L., 2007. Effects of genes, sex, age, and activity on BMC, bone size, and areal and volumetric BMD. Journal of Bone and Mineral Research 22, 737-746.

Herries, A.I.R., Curnoe, D., Adams, J.W., 2009. A multi-disciplinary seriation of early *Homo* and *Paranthropus* bearing palaeocaves in Southern Africa. Quaternary International 202, 14-28.

Huiskes, R., 2000. If bone is the answer, then what is the question? Journal of Anatomy 197, 145-56.

Jashashvili, T., Dowdeswell, M.R., Lebrun, R., Carlson, K.J., 2015. Cortical structure of hallucal metatarsals and locomotor adaptations in hominoids. PLoS One 10, e0117905.

Johansson, J., Nordström, A., Nordström, P., 2015. Objectively measured physical activity is associated with parameters of bone in 70-year-old men and women. Bone 81, 72-79.

Judex, S., Garman, R., Squire. M, Leah-Rae, D., Rubin, C., 2004. Genetically based influences on the site-specific regulation of trabecular and cortical bone morphology. Journal of Bone and Mineral Research 19, 600-606.

Kibii, J.M., Churchill, S.E., Schmid, P., Carlson, K.J., Reed, N.D., de Ruiter, D.J., Berger, L.R., 2011. A partial pelvis of *Australopithecus sediba*. Science 333, 1407-1411.

Kivell, T.L., 2016. A review of trabecular bone functional adaptation: What have we learned from trabecular analyses in extant hominoids and what can we apply to fossils? Journal of Anatomy 228, 569-594.

Komza, K., Skinner, M.M., 2019. First metatarsal trabecular bone structure in extant hominoids and Swartkrans hominins. Journal of Human Evolution 131, 1-21.

L'Abbé, E.N., Loots, M., Meiring, J.H., 2005. The Pretoria Bone Collection: A modern South African skeletal sample. Homo 56, 197-205.

Lanyon, L., Skerry, T., 2001. Perspective: Postmenopausal osteoporosis as a failure of bone's adaptation to functional loading: A hypothesis. Journal of Bone and Mineral Research 16, 1937-1947.

Lieberman, D.E., Pearson, O.M., Polk, J.D., Demes, B., Crompton, A.W., 2003. Optimization of bone growth and remodeling in response to loading in tapered mammalian limbs. Journal of Experimental Biology 206, 3125-3138.

Lieberman, D.E., Polk, J.D., Demes, B., 2004. Predicting long bone loading from cross-sectional geometry. American Journal of Physical Anthropology 123, 156-171.

Lotz, J.C., Cheal, E.J., Hayes, W.C., 1995. Stress distributions within the proximal femur during gait and falls: Implications for osteoporotic fracture. Osteoporosis International 5, 252-261.

Lovejoy, C.O., 1975. Biomechanical perspectives on the lower limb of early hominids. In: Tuttle, R.H. (Ed.), Primate Functional Morphology and Evolution. Mouton, Paris, pp. 291-326.

Lovejoy, C.O., 1988. Evolution of human walking. Scientific American 259, 118-125.

Lovejoy, C.O., 2005. The natural history of human gait and posture. Part 2. Hip and thigh. Gait & Posture 21, 113-124.

Lovejoy, C.O., Cohn, M.J., White, T.D., 1999. Morphological analysis of the mammalian postcranium: A developmental perspective. Proceedings of the National Academy of Sciences USA 96, 13247-13252.

Lovejoy, C.O., Heiple, K.G., Burstein, A.H., 1973. The gait of *Australopithecus*. American Journal of Physical Anthropology 38, 757-780.

Lovejoy, C.O., Meindl, R.S., Ohman, J.C., Heiple, K.G., White, T.D., 2002. The Maka femur and its bearing on the antiquity of human walking: Applying contemporary concepts of morphogenesis to the human fossil record. American Journal of Physical Anthropology 119, 97-133.

Lovejoy, C.O., Suwa, G., Spurlock, L., Asfaw, B., White, T., 2009. The pelvis and femur of *Ardipithecus ramidus*: The emergence of upright walking. Science 326, 71e1-71e6.

Macchiarelli, R., Bondioli, L., Galichon, V., Tobias, P.V., 1999. Hip bone trabecular architecture shows uniquely distinctive locomotor behaviour in South African australopithecines. Journal of Human Evolution 36, 211-232.

Marchi, D., Walker, C.S., Wei, P., Holliday, T.W., Churchill, S.E., Berger, L.R., DeSilva, J. M., 2016. The thigh and leg of *Homo naledi*. Journal of Human Evolution 30, 1-31.

MathWorks, 2013. MATLAB and Statistics Toolbox Release, 2013. Version 8.1. The MathWorks, Inc., Natick. https://fr.mathworks.com/.

McHenry, H.M., 1975. Biomechanical interpretation of the early hominid hip. Journal of Human Evolution 4, 343-355.

Meyer, F., Beucher, S., 1990. Morphological segmentation. Journal of Visual Communication and Image Representation 1, 21-46.

Mittra, E., Rubin, C., Qin, Y.X., 2005. Interrelationship of trabecular mechanical and microstructural properties in sheep trabecular bone. Journal of Biomechanics 38, 1229-1237.

Morimoto, N., Ponce de León, M.S., Zollikofer, C.P.E., 2011. Exploring femoral diaphyseal shape variation in wild and captive chimpanzees by means of morphometric mapping: A test of Wolff's Law. The Anatomical Record 294, 589-609.

Morris, A.G., 1984. Osteological analysis populations of the Cape and Western Africa. Ph.D. Dissertation, University of the Witwatersrand, Johannesburg.

Napier, J.R., 1964. The evolution of bipedal walking in the hominids. Archives de Biologie (Liege) 75, 673-708.

Ohman, J.C., Krochta, T.J., Lovejoy, C.O., Mensforth, R.P., Latimer, B., 1997. Cortical bone distribution in the femoral neck of hominoids: Implications for the locomotion of *Australopithecus afarensis*. American Journal of Physical Anthropology 104, 117-131.

O'Neill, M.C., Dobson, S.D., 2008. The degree and pattern of phylogenetic signal in primate long-bone structure. Journal of Human Evolution 54, 309-322.

Pearson, O.M., Lieberman, D.E., 2004. The aging of Wolff's "law": Ontogeny and responses to mechanical loading in cortical bone. Yearbook of Physical Anthropology 47, 63-99.

Pebesma, E.J., 2004. Multivariable geostatistics in S: The gstat package. Computers & Geosciences 30, 683-691.

Pickering, R., Kramers, J.D., Hancox, P.J., de Ruiter, D.J., Woodhead, J.D., 2011. Contemporary flowstone development links early hominin bearing cave deposits in South Africa. Earth and Planetary Science Letters 306, 23-32.

Pickering, T.R., Heaton, J.L., Clarke, R.J., Sutton, M.B., Brain, C.K., Kuman, K., 2012. New hominid fossils from Member 1 of the Swartkrans formation, South Africa. Journal of Human Evolution 62, 618-628.

Pickering, R., Herries, A.I.R., Woodhead, J.D., Hellstrom, J.C., Green, H.E., Paul, B., Ritzman, T., Strait, D.S., Schoville, B.J., Hancox, P.J., 2019. U-Pb-dated flowstones restrict South African early hominin record to dry climate phases. Nature 565, 226-229.

Puymerail, L., Ruff, C.B., Bondioli, L., Widianto, H., Trinkaus, E., Macchiarelli, R., 2012. Structural analysis of the Kresna 11 *Homo erectus* femoral shaft (Sangiran, Java). Journal of Human Evolution 63, 741-749.

R Core Team, 2018. R: A language and environment for statistical computing. R Foundation for Statistical Computing, Vienna. http://www.R-project.org/.

Rafferty, K.L., 1998. Structural design of the femoral neck in primates. Journal of Human Evolution 34, 361-383.

Raichlen, D.A., Gordon, A.D., Foster, A.D., Webber, J.T., Sukhdeo, S.M., Scott, R.S., Gosman, J.H., Ryan, T.M., 2015. An ontogenetic framework linking locomotion and trabecular bone architecture with applications for reconstructing hominin life history. Journal of Human Evolution 81, 1-12.

Robinson, J.T., 1972. Early Hominid Posture and Locomotion. University of Chicago Press, Chicago.

Roerdink, J., Meijster, A., 2000. The watershed transform: Definitions, algorithm and parallelization strategies. Fundamenta Informaticae 41, 178-228.

Ruff, C.B., 1995. Biomechanics of the hip and birth in early *Homo*. American Journal of Physical Anthropology 98, 527-574.

Ruff, C.B., 2010. Body size and body shape in early hominins. Implications of the Gona pelvis. Journal of Human Evolution 58, 166-178.

Ruff, C.B., 2017. Mechanical constraints on the hominin pelvis and the "obstetrical dilemma". The Anatomical Record 30, 946-955.

Ruff, C.B., Higgins, R., 2013. Femoral neck structure and function in early hominins. American Journal of Physical Anthropology 150, 512-525.

Ruff, C.B., McHenry, H.M., Thackeray, J.F., 1999. Cross-sectional morphology of the SK 82 and 97 proximal femora. American Journal of Physical Anthropology 109, 509-521.

Ruff, C.B., Holt, B.H., Trinkaus, E., 2006. Who's afraid of the big bad Wolff?: "Wolff's Law" and bone functional adaptation. American Journal of Physical Anthropology 129, 484-498.

Ruff, C.B., Burgess, M.L., Ketcham, R.A., Kappelman, J., 2016. Limb bone structural proportions and locomotor behavior in AL 288-1 ("Lucy"). PLoS One 11, e0166095.

Ruff, C.B., Burgess, M.L., Squyres, N., Junno, J.A., Trinkaus, E., 2018. Lower limb articular scaling and body mass estimation in Pliocene and Pleistocene hominins. Journal of Human Evolution 115, 85-111.

Ryan, T.M., Sukhdeo, S., 2016. KSD-VP-1/1: Analysis of the postcranial skeleton using high-resolution computed tomography. In: Haile-Selassie, Y., Su, D.E. (Eds), The Postcranial Anatomy of *Australopithecus afarensis*. Springer, Dordrecht, pp. 39-62.

Ryan, T.M., Carlson, K.J., Gordon, A.D., Jablonski, N. Shaw, C.N., Stock, J.T., 2018. Human-like hip joint loading in *Australopithecus africanus* and *Paranthropus robustus*. Journal of Human Evolution. https://doi.org/10.1016/j.jhevol.2018.03.008.

Scilab Enterprises, 2017. Scilab: Free and open source software for numerical computation (OS, Version 4.1.2). http://www.scilab.org.

Shaw, C., Ryan, T., 2012. Does skeletal anatomy reflect adaptation to locomotor patterns? Cortical and trabecular architecture in human and nonhuman anthropoids. American Journal of Physical Anthropology 147, 187-200.

Shimizu, D., Gunji, H., Hashimoto, H., Hosaka, K., Huffman, M.A., Matsumoto-Oda, A., Kawanaka, K., Nishida, T., 2002. The four chimpanzee skulls collected in the Mahale Mountains, Tanzania. Anthropological Science 110, 251-266.

Simpson, S.W., Levin, N.E., Quade, J., Rogers, M.J., Semaw, S., 2019. *Ardipithecus ramidus* postcrania from the Gona Project area, Afar Regional State, Ethiopia. Journal of Human Evolution 129, 1-45.

Skerry, T.M., 2008. The response of bone to mechanical loading and disuse: Fundamental principles and influences on osteoblast/osteocyte homeostasis. Archives of Biochemistry and Biophysics 473, 117-123.

Stern, J.T., 2000. Climbing to the top: A personal memoir of *Australopithecus afarensis*. Evolutionary Anthropology 9, 113-133.

Stern, J.T., Susman, R.L., 1981. Electromyography of the gluteal muscles in *Hylobates*, *Pongo*, and *Pan*: Implications for the evolution of hominid bipedality. American Journal of Physical Anthropology 55, 153-166.

Su, A., Carlson, K.J., 2017. Comparative analysis of trabecular bone structure and orientation in South African hominin tali. Journal of Human Evolution 106, 1-18.

Susman, R.L., de Ruiter, D., Brain, C.K., 2001. Recently identified postcranial remains of *Paranthropus* and early *Homo* from Swartkrans Cave, South Africa. Journal of Human Evolution 41, 607-629.

Tague, R.G., Lovejoy, C.O., 1986. The obstetric pelvis of A.L. 288-1 (Lucy). Journal of Human Evolution 15, 237-255.

Vansickle, C., 2017. Measuring lateral iliac flare by different methods risks obscuring evolutionary changes in the pelvis. The Anatomical Record 300, 956-963.

Videan, E.N., McGrew, W.C., 2001. Are bonobos (*Pan paniscus*) really more bipedal than chimpanzees (*Pan troglodytes*)? American Journal of Primatology 54, 233-239.

Vrba, E.S., 1975. Some evidence of chronology and palaeoecology of Sterkfontein, Swartkrans and Kromdraai from the fossil Bovidae. Nature 254, 301-304.

Wallace, I.J., Tommasini, S.M., Judex, S., Garland, T., Demes, B., 2012. Genetic variations and physical activity as determinants of limb bone morphology: An experimental approach using a mouse model. American Journal of Physical Anthropology 148, 24-35.

Ward, C.V., 2002. Interpreting the posture and locomotion of *Australopithecus afarensis*: Where do we stand? American Journal of Physical Anthropology 119, 185-215.

Ward, C.V., 2013. Postural and locomotor adaptations of *Australopithecus* species. In: Reed, K.E., Fleagle, J.G., Leakey, R.E. (Eds), The Paleobiology of *Australopithecus*. Springer, Dordrecht, pp. 235-245.

Wood, S.N., 2006. Generalized Additive Models: An Introduction with R. Chapman & Hall, Boca Raton.

Zanolli, C., Pan, L., Dumoncel, J., Kullmer, O., Kundrát, M., Liu, W., Macchiarelli, R., Mancini, L., Schrenk, F., Tuniz, C., 2018. Inner tooth morphology of *Homo erectus* from Zhoukoudian. New evidence from an old collection housed at Uppsala University, Sweden. Journal of Human Evolution 116, 1-13.

Zeininger, A., Patel, B.A., Zipfel, B., Carlson, K.J., 2016. Trabecular architecture in the StW 352 fossil hominin calcaneus. Journal of Human Evolution 97, 145-158.

Captions to the figures

Figure 1. The four proximal femora of *Paranthropus robustus* from Swartkrans considered in this study. All specimens shown in anterior view.

Figure 2. µXCT-based virtual rendering in semitransparency of four proximal femora in anterior view of *Paranthropus robustus* from Swartkrans (SK 82, SK 97, SK 3121, and SWT1/LB-2) and of an extant human and chimpanzee representatives with location of base of neck (a) and mid-neck (b) slices used to measure cortical thickness (cf. Ruff and Higgins, 2013:Fig. 3). Note that only the mid-neck section has been considered in SK 3121.

Figure 3. Examples of cortical bone thickness measurements assessed on a virtual slice perpendicular to the longitudinal axis of the femoral neck of SK 82: a) most superior (L1) and most inferior (L2) limits of the periosteal perimeter and corresponding superoinferior and anteroposterior orthogonal axes; b) orthogonal axes set at 45° with respect to the superoinferior axis delimiting the superior (S), inferior (I), anterior (A) and posterior (P) quadrants; c) cortical bone thicknesses measured between each pixel of the outer (periosteal) contour of the neck section and the smallest distance to the endosteal contour.

Figure 4. µXCT-based virtual sections perpendicular to the longitudinal neck axis and their associated cortical binary masks taken at the base of neck (upper) and at mid-neck (lower) in four *Paranthropus robustus* specimens from Swartkrans (SK 82, SK 97, SK 3121, and SWT1/LB-2) and in an extant human and chimpanzee representatives. Note that only the mid-neck section has been considered in SK 3121.

Figure 5. Lateral-to-medial variation from the base of neck (0%) to the head-neck junction (100%) of the S/I ratio between the superior (S) and inferior (I) cortical thicknesses in: a) *Paranthropus robustus* (SK 82: solid line; SK 97: dotted line); b) extant humans (n = 25); c) chimpanzees (n = 8). In extant humans and chimpanzee, the mean (central line) ± 1 SD are provided.

Figure 6. Lateral-to-medial variation from the base of neck (0%) to the head-neck junction (100%) of the mean cortical thickness (in mm) distinctly assessed for the anterior (solid lines) and posterior (dotted lines) quadrants (cf. Fig. 3) of the femoral neck in: a) SK 82; b) SK 97; c) SWT1/LB-2 (anterior quadrant only); d, e) extant humans (n = 25) anterior (d) and posterior (e) walls; f, g) chimpanzee (n = 8) anterior (f) and posterior (g) walls. In extant humans and chimpanzees, the mean (central line) ± 1 SD are provided.

Figure 7. µXCT-based morphometric map of the virtually unzipped, unrolled and projected cortical bone thickness of the *Paranthropus robustus* SK 82 femoral neck from the base of neck (bottom Y-axis) to the head-neck junction (top Y-axis) compared to the consensus cartographies generated for the extant human (n = 25) and chimpanzee (n = 8) samples. Relative thickness is rendered by a pseudocolor scale increasing from dark blue (0, thinner) to red (1, thicker). Abbreviations: ant. = anterior quadrant; inf. = inferior quadrant; post. = posterior quadrant; sup. = superior quadrant.

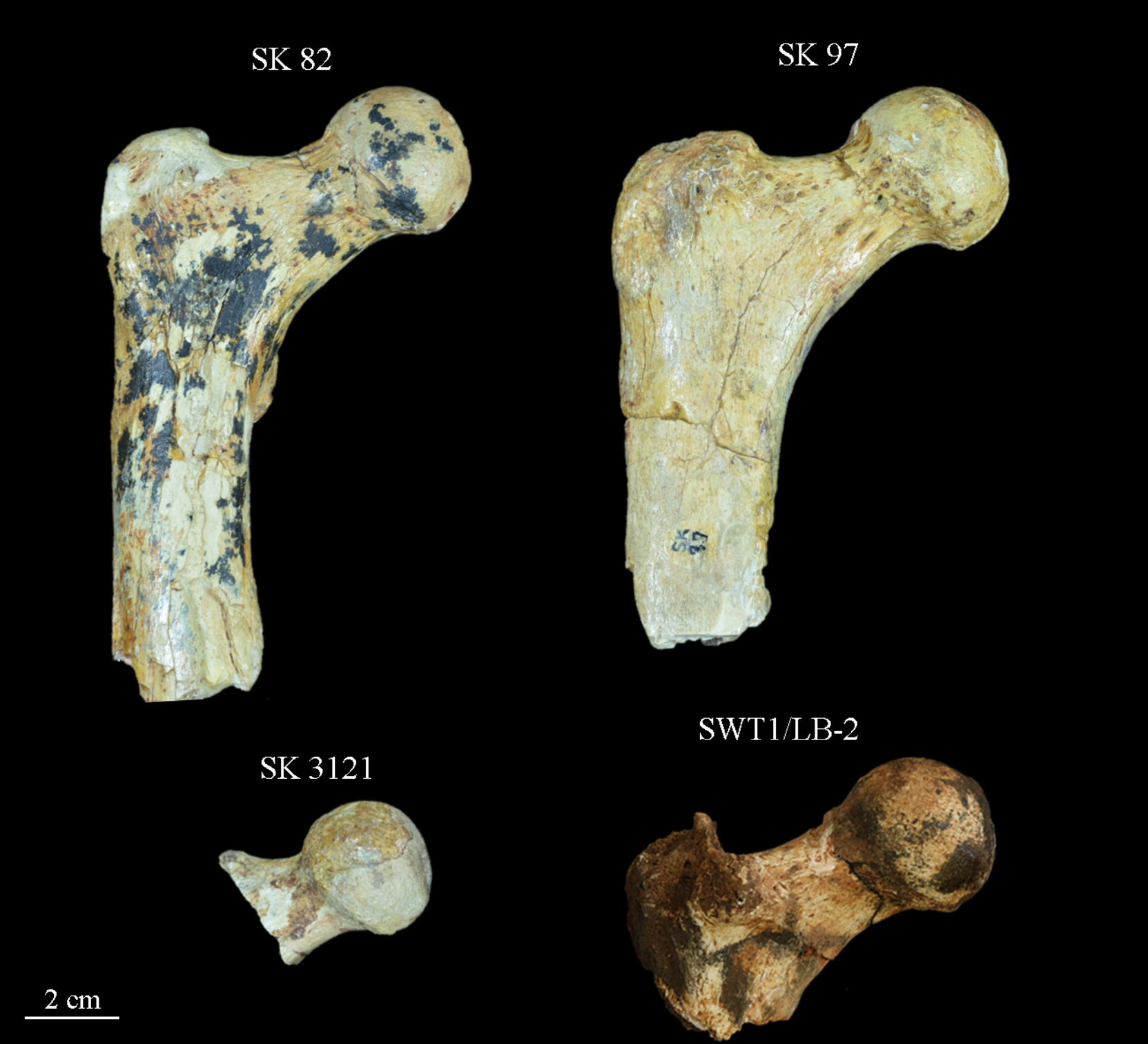
SK 82
SK 97
SK 3121
SWT1/LB-2
2 cm

SK 82

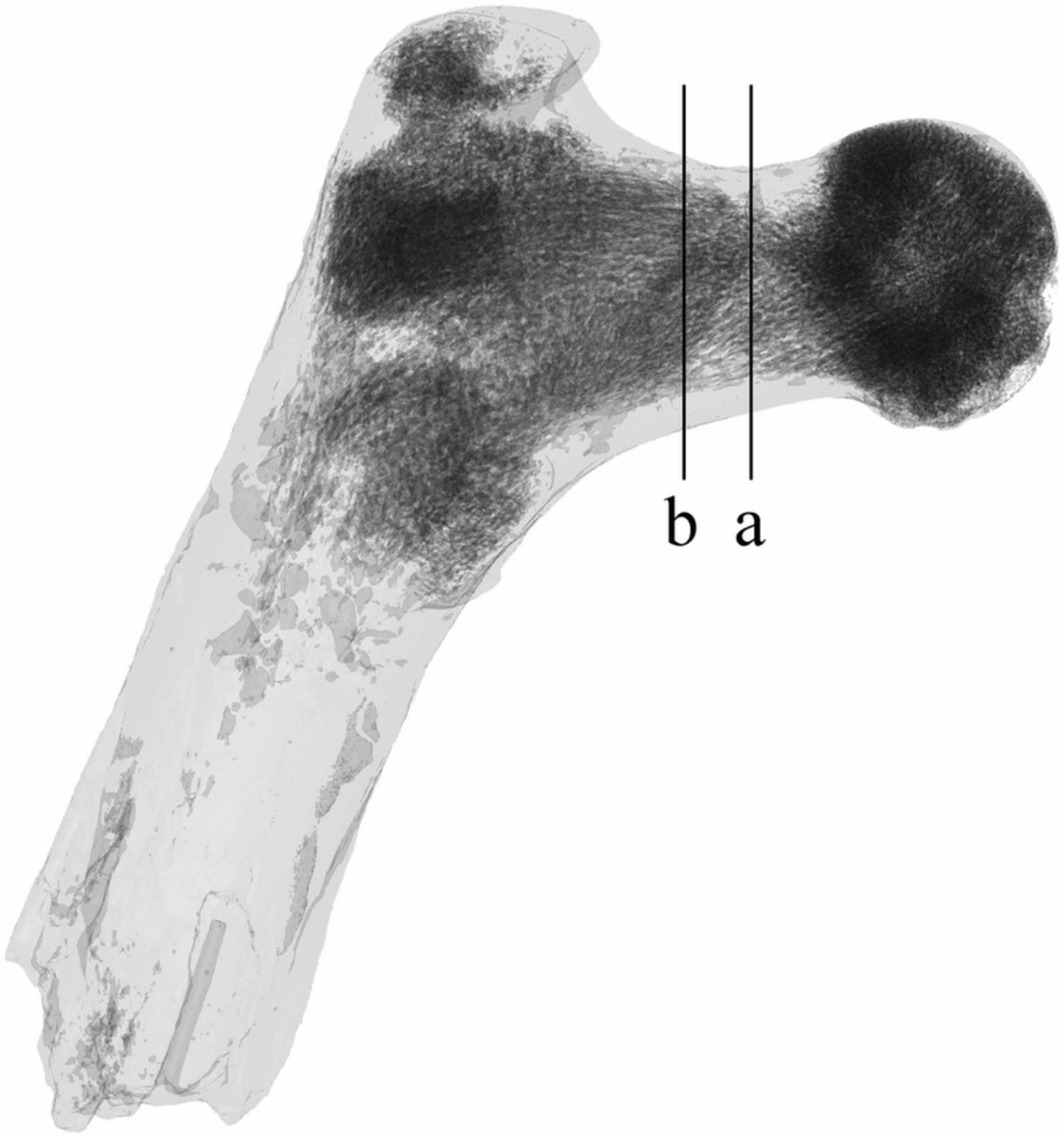

SK 97

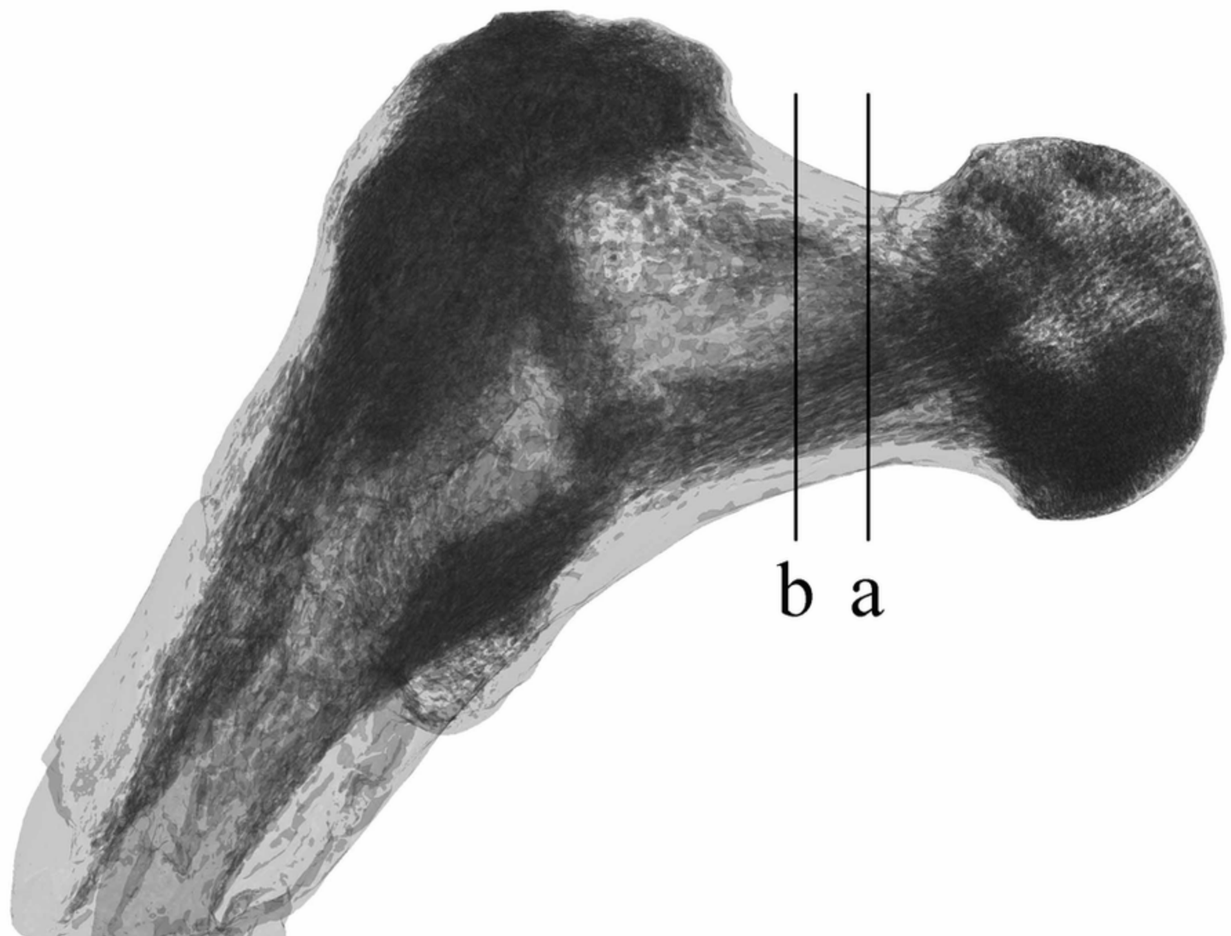

extant human

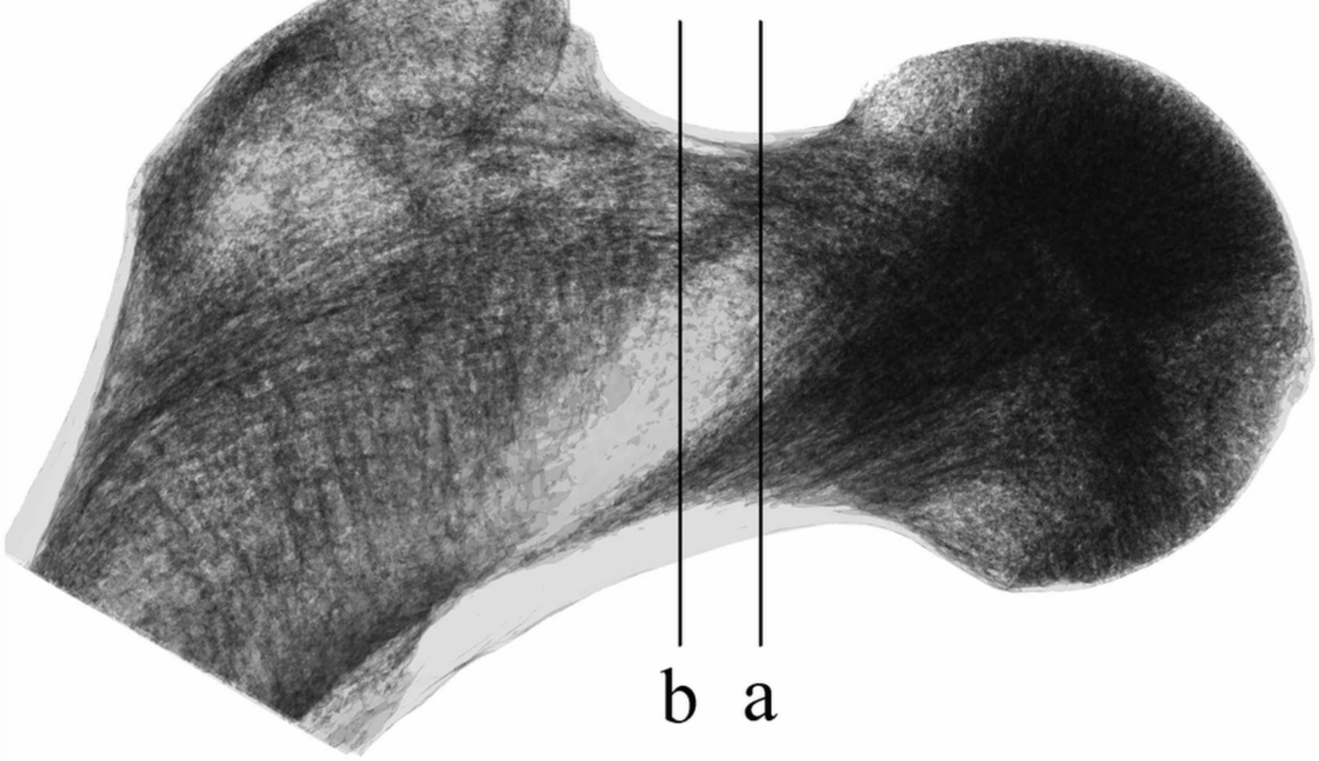

SK 3121

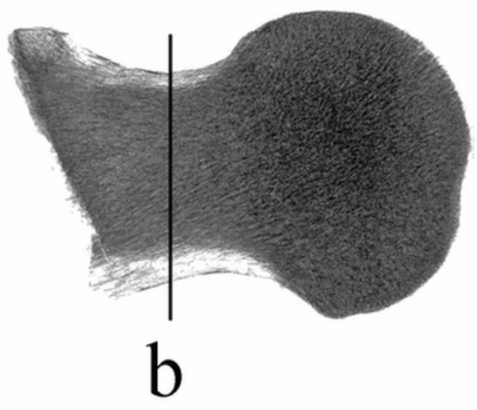

SKWT1/LB-2

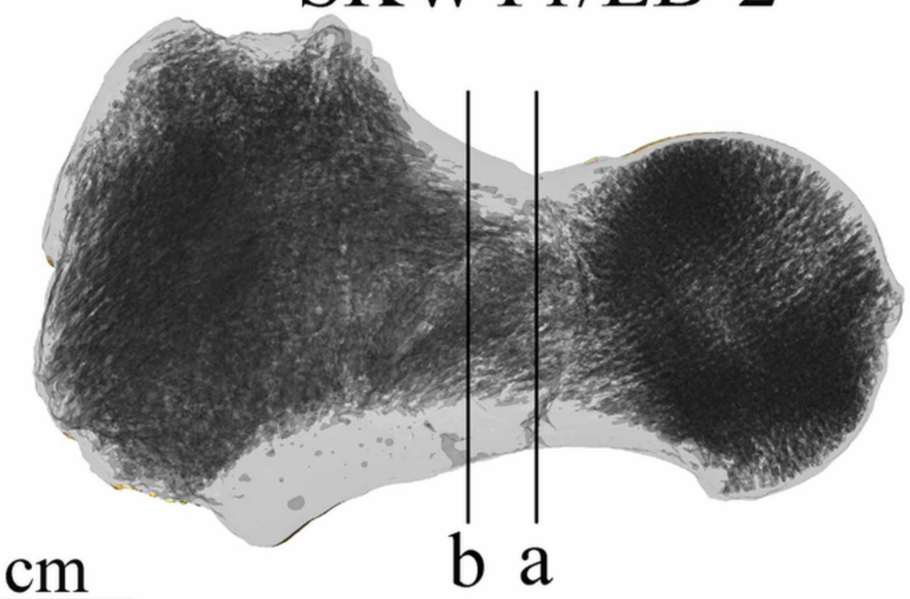

Pan troglodytes

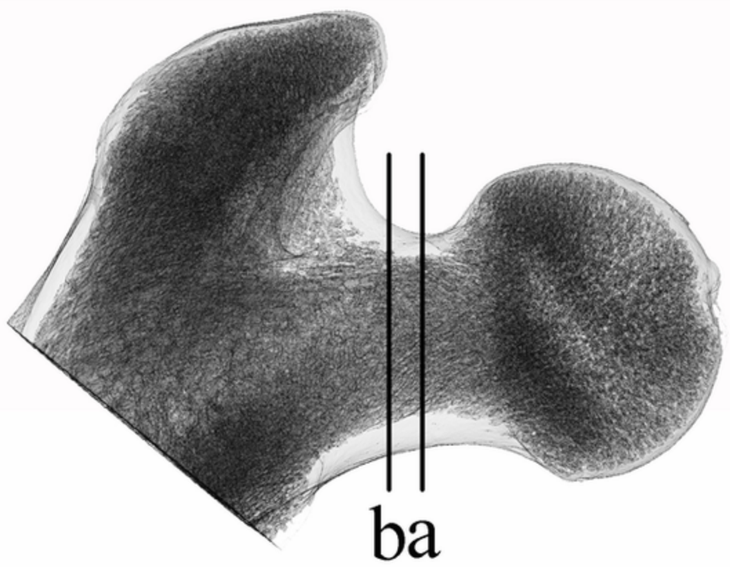

2 cm

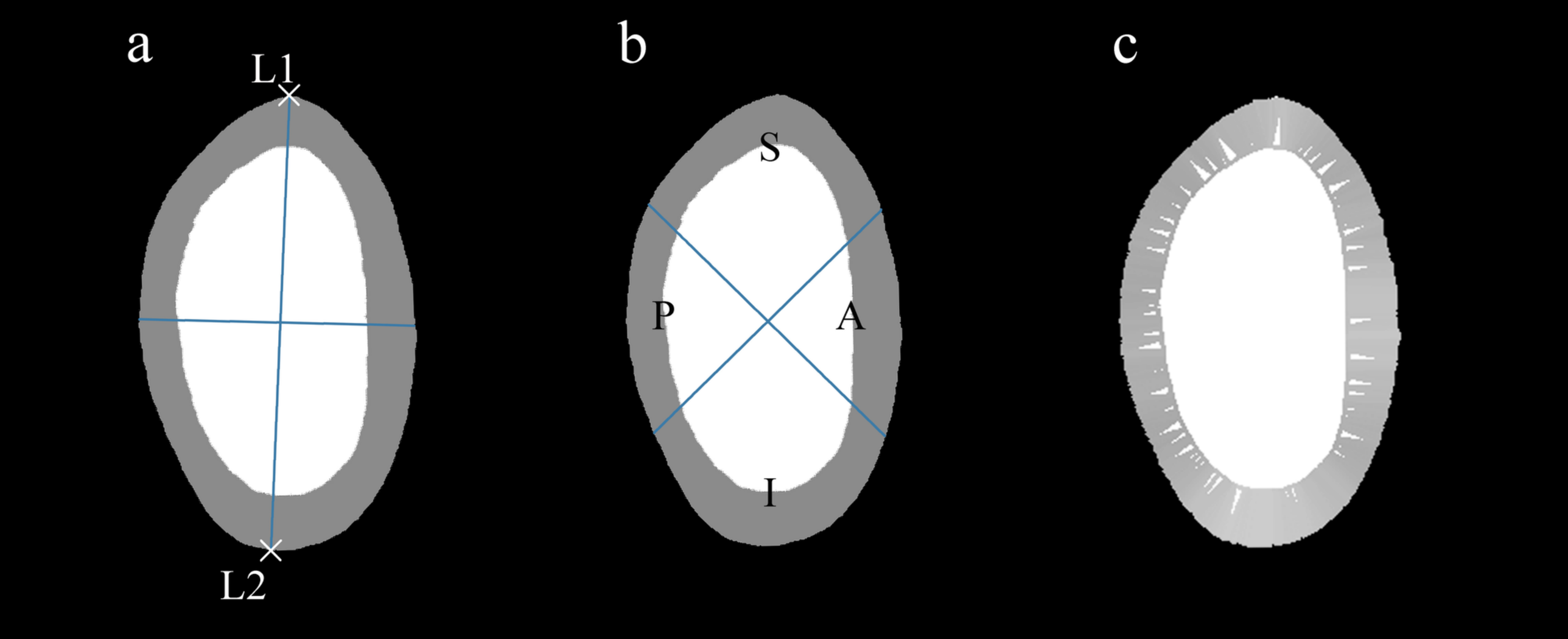
a
L1
L2
b
S
P
A
I
c

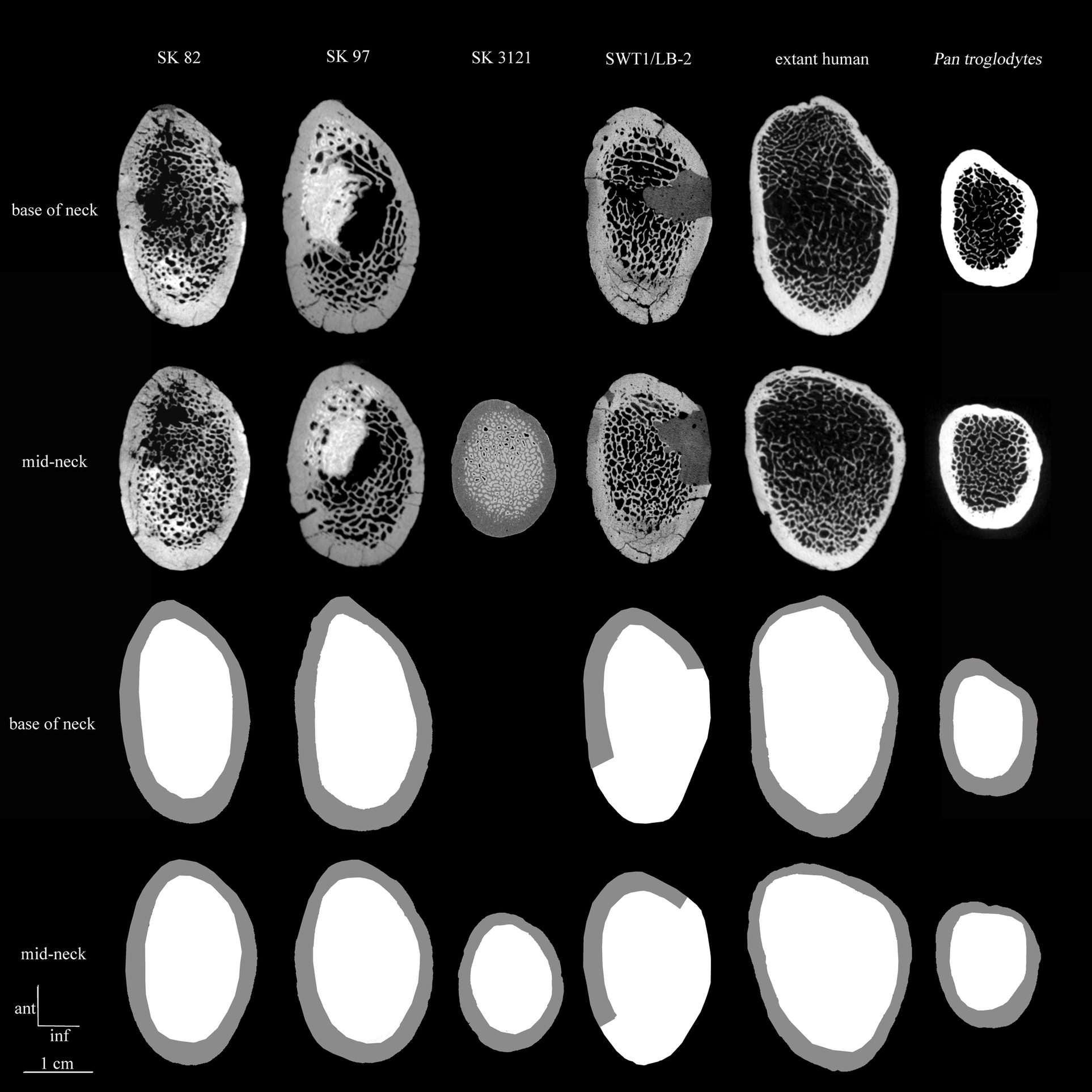
SK 82
SK 97
SK 3121
SWT1/LB-2
extant human
Pan troglodytes
base of neck
mid-neck
base of neck
mid-neck
ant
inf
1 cm

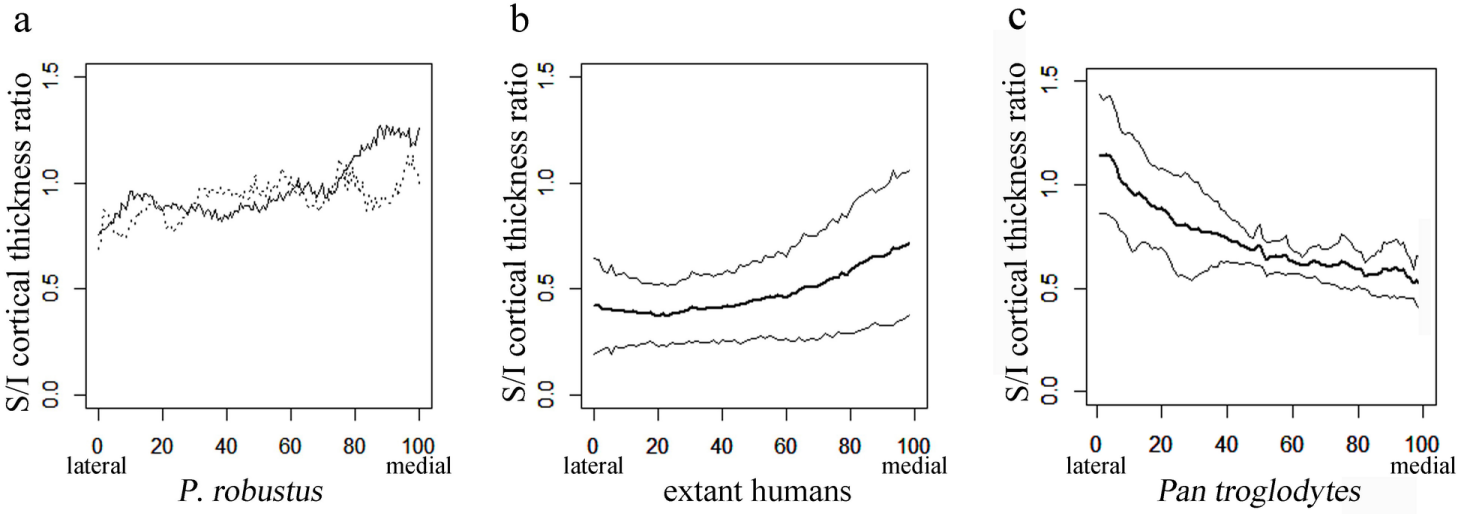
a
S/I cortical thickness ratio
0.0
0.5
1.0
1.5
0
20
40
60
80
100
lateral
medial
P. robustus
b
S/I cortical thickness ratio
0.0
0.5
1.0
1.5
0
20
40
60
80
100
lateral
medial
extant humans
c
S/I cortical thickness ratio
0.0
0.5
1.0
1.5
0
20
40
60
80
100
lateral
medial
Pan troglodytes

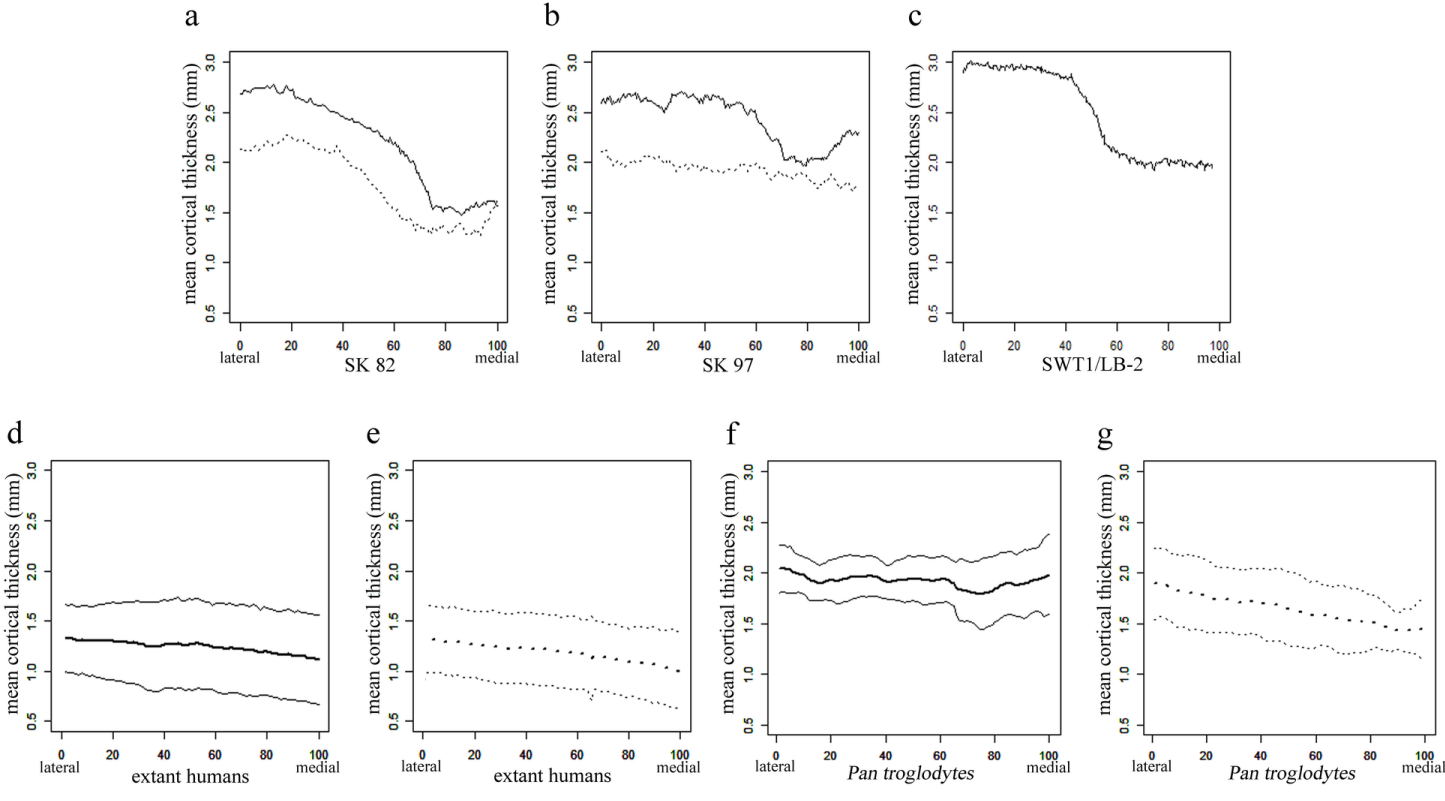
a
b
c
d
e
f
g
mean cortical thickness (mm)
0.5
1.0
1.5
2.0
2.5
3.0
0
20
40
60
80
100
lateral
medial
SK 82
SK 97
SWT1/LB-2
extant humans
extant humans
Pan troglodytes
Pan troglodytes

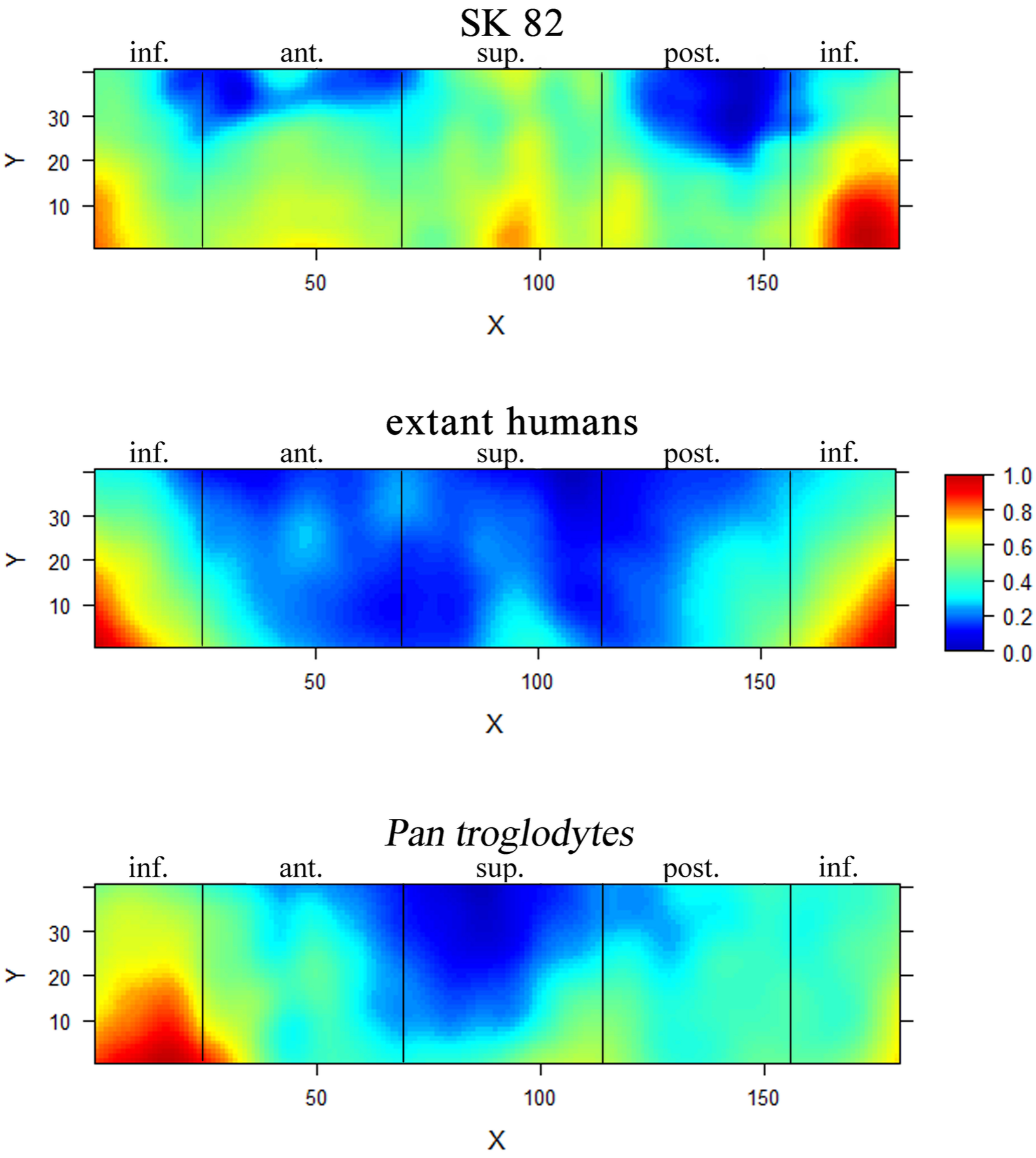
SK 82
inf.
ant.
sup.
post.
inf.
Y
30
20
10
50
100
150
X
extant humans
inf.
ant.
sup.
post.
inf.
Y
30
20
10
50
100
150
X
1.0
0.8
0.6
0.4
0.2
0.0
Pan troglodytes
inf.
ant.
sup.
post.
inf.
Y
30
20
10
50
100
150
X

Table 1

Cortical bone thickness (in mm) of the superior (S) and inferior (I) cortices and S/I ratios assessed at the base of neck and at mid-neck, and mean cortical thickness (in mm) and S/I ratios assessed for the entire superior and inferior neck quadrants in *Paranthropus robustus* from Swartkrans (SK 82, SK 97, SK 3121 and SWT1/LB-2) and in a comparative sample of extant humans (n = 25; SD within parentheses) and *Pan troglodytes* (n = 8; SD within parentheses). For the linear measures, the values available for the *Australopithecus afarensis* A.L. 288-1 femoral neck are also shown. Italics indicates XCT-based measures; all remaining values are µXCT-based data from the present study.

		Cortical thickness						Mean cortical thickness					
		Base of neck			Mid-neck			Base of neck			Mid-neck		
Specimen	Taxon	Superior	Inferior	S/I	Superior	Inferior	S/I	Superior	Inferior	S/I	Superior	Inferior	S/I
SK 82	*P. robustus*	2.59–*1.93*[a]	3.43–*4.09*[a]	0.76–*0.47*[a]	2.42–*3.00*[a]	2.80–*2.86*[a]	0.86–*1.05*[a]	2.20	2.84	0.78	2.32	2.41	0.96
SK 97	*P. robustus*	2.30–*1.18*[a]	3.37–*2.83*[a]	0.68–*0.42*[a]	2.81–*1.50*[a]	2.94–*2.20*[a]	0.96–*0.68*[a]	1.83	3.05	0.60	2.18	2.87	0.76
SK 3121	*P. robustus*				1.80	2.50	0.71				1.76	2.64	0.67
SWT1/LB-2	*P. robustus*	1.99			2.82			2.45			2.54		
	extant humans	1.21 (0.52)	3.42 (1.12)	0.37 (0.13)	1.11 (0.49)	2.48 (0.68)	0.48 (0.17)	1.02 (0.30)	2.58 (0.83)	0.46 (0.23)	0.96 (0.35)	1.99 (0.52)	0.50 (0.15)
	Pan troglodytes	2.86 (1.18)	2.75 (0.42)	1.02 (0.32)	1.62 (0.42)	2.50 (0.52)	0.66 (0.13)	2.40 (0.55)	2.57 (0.33)	0.93 (0.12)	1.75 (0.35)	2.38 (0.46)	0.74 (0.07)
A.L. 288-1[b]	*A. afarensis*	1.20	3.50	0.34	1.50	2.60	0.58						

[a] Ruff and Higgins (2013).

[b] Ruff (2018, pers. comm.; see also Ruff et al., 2016:Fig. 7).

Table 2

Mean cortical bone thickness (in mm) assessed for the entire anterior (A) and posterior (P) quadrants at the base of neck and at mid-neck in *Paranthropus robustus* from Swartkrans (SK 82, SK 97 and SWT1/LB-2) and in a comparative sample of extant humans (n = 25; min-max values within parentheses) and *Pan troglodytes* (n = 8; min-max values within parentheses).

		Base of neck		Mid-neck	
		Anterior	Posterior	Anterior	Posterior
SK 82	*P. robustus*	2.68	2.13	2.34	1.82
SK 97	*P. robustus*	2.59	2.11	2.55	1.93
SWT1/LB-2	*P. robustus*	2.90		2.55	
	extant humans	1.39 (0.64–2.18)	1.32 (0.68–2.00)	1.31 (0.60–1.99)	1.24 (0.61–1.81)
	Pan troglodytes	2.28 (1.87–2.67)	2.08 (1.63–2.61)	2.14 (1.72–2.51)	1.84 (1.26–2.39)